16. Computed Tomography

Thorsten M. Buzug

In this chapter, historical milestones of computed tomography (CT) (Sect. 16.2), recent technology with a focus on generation and detection of x-rays (Sect. 16.3), as well as image reconstruction (Sect. 16.4) are discussed. Furthermore, the chapter includes aspects of applications (Sect. 16.5), dose exposure in computed tomography (Sect. 16.6), and a brief overview on special CT developments (Sect. 16.7). Since this chapter gives a review, the interested reader is referred to recent literature on computed tomography including a detailed discussion of CT technology in the references section.

16.1 Background

Research in computed tomography is still as exciting as at the beginning of its development during the 1960s and 1970s; however, several competing methods exist, the most important being magnetic resonance imaging (MRI). Since the invention of MRI during the 1980s, the phasing out of CT has been anticipated. Nevertheless, to date, the most widely used imaging technology in radiology departments is still CT. Although MRI and positron emission tomography (PET) have been widely installed in radiology and nuclear medicine departments, the term tomography is clearly associated with x-ray computed tomography. In the USA, computed tomography is also called computerized axial tomography (CAT).

Computed tomography has evolved into an indispensable imaging method in clinical routine. It was the first method to noninvasively acquire images of the inside of the human body that were not biased by superposition of distinct anatomical structures [16.1–4]. This is due to the projection of all the information into a two-dimensional imaging plane, as typically seen in planar x-ray fluoroscopy. Therefore, CT yields images of much higher contrast compared with conventional radiography. During the 1970s, this was an enormous

step toward the advance of diagnostic possibilities in medicine.

Some hospitals have actually replaced their conventional shock rooms with a CT-based virtual shock room. In this scenario, imaging and primary care of the patient takes place using a CT scanner equipped with anesthesia devices. In a situation where fast three-dimensional imaging of a trauma patient is necessary (and it is unclear whether MRI is an adequate imaging method in terms of compatibility with the patient), computed tomography is the standard imaging modality. Additionally, due to its ease of use, clear interpretation in terms of physical attenuation values, progress in detector technology, reconstruction mathematics, and reduction of radiation exposure, computed tomography will maintain and expand its established position in radiology.

Recently, interesting technical, anthropomorphic, forensic, and archeological as well as paleontological applications of computed tomography have been developed. These applications further strengthen the method as a generic diagnostic tool for nondestructive material testing and three-dimensional visualization beyond its medical uses. Magnetic resonance imaging fails whenever the object to be examined is dehydrated. In these circumstances, computed tomography is the three-dimensional imaging method of choice.

Today, whole-body scans as well as imaging of very small vessels, for instance, vessels of the feet, belong to clinical routine (Fig. 16.1). Furthermore, the preoperatively acquired CT image stack can be used to synthetically compute projections for any given angulations. A surgeon can use this information to get an impression of the images that are taken intraoperatively by a C-arm image intensifier. Therefore, there is no need to acquire additional radiographs and the artificially generated projection images actually resem-

Fig. 16.1 Whole-body scans can be performed with the latest generation of CT systems, including multislice detector systems. Even very small vessels of the feet can be precisely visualized (courtesy Philips Medical Systems)

ble conventional radiographs. Additionally, the German Employer's Liability Insurance Association insists on a CT examination in severe accidents that occur at work. Therefore, CT has advanced to become the standard diagnostic imaging modality in trauma clinics. Patients with heavy trauma, fractures, and luxations benefit greatly from the clarification provided by imaging techniques such as computed tomography.

16.2 Milestones of Computed Tomography

Conventional x-ray imaging suffers from the severe drawback that it only produces two-dimensional projections of a three-dimensional object. This results in a reduction in spatial information (although an experienced radiologist might be able to compensate for this). In any case, a projection represents an averaging. The result of the averaging can be imagined if one were to overlay several radiographic sections on the light box for diagnosis. It would be difficult for even an expert to interpret the results, as averaging comes along with a considerable reduction in contrast, compared with the contrast present in one slice.

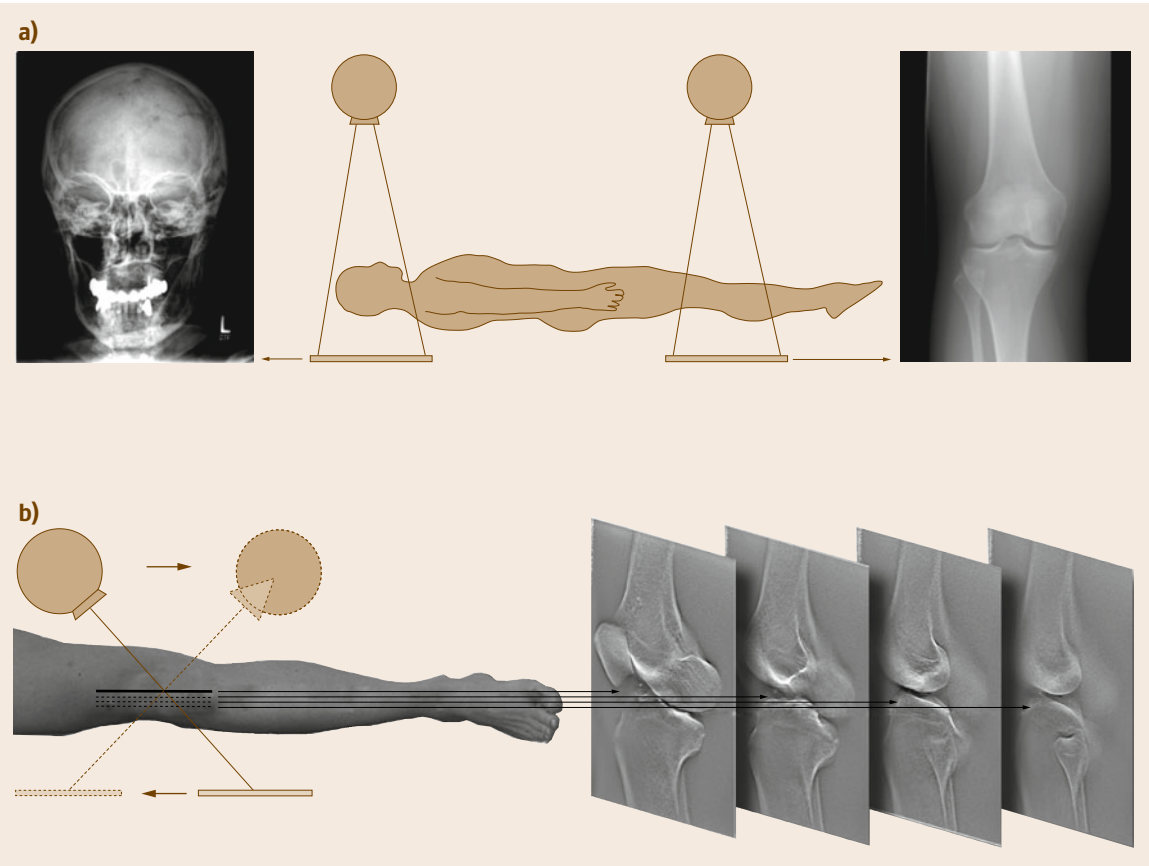

Fig. 16.2a,b Conventional planar x-ray leads to low-contrast images that do not allow clinical diagnostics involving soft tissue **(a)**. The figure shows the cranial bone (*left*), in which details of spatial structures in the brain cannot be recognized. In the image of the knee (*right*), even bone structures have low contrast. This low contrast is caused by the averaging process during the x-rays' passage through the body. The first attempts to create radiographic slices of the human body were carried out using conventional or analog geometric tomography, also referred to as tomosynthesis if the acquired x-ray images are digitally postprocessed **(b)**

Figure 16.2a shows conventional images of the cranium (left) and of the knee (right). These images show the high attenuation of x-rays within, for example, the cranial bone and most notably around the dental fillings. The small differences in attenuation that characterize soft tissue, however, are not visible at all. The morphology of the brain, in particular, is completely lost in the averaging process. In the knee, even the bone structures are imaged with poor contrast due to the superimposition.

16.2.1 Analog Geometric Tomography and Tomosynthesis

In the 1920s, the desire to undo the averaging process that characterizes conventional x-ray radiography led to the first tomographic concept. The word "tomography" itself is composed of two Greek words: *tomos* (slice) and *graphein* (draw). The use of the word "tomography" was considerably influenced by the Berlin physician *Grossmann*, whose Grossmann tomograph was able to image one single slice of the body [16.5].

The principle of the conventional or analog geometric tomography method is illustrated in Fig. 16.2b. During image acquisition, the x-ray tube is moved linearly in one direction, while the x-ray film is synchronously moved in the opposite direction. For this reason, only points in the plane of the center of rotation are imaged sharply. All points above and below this region are blurred, more so at greater distances from the center of rotation. Hence, this method can be interpreted as *blurring tomography*. It is called *tomosynthesis* if there is digital postprocessing of the projection images.

The blurred information above and below the center of rotation does not disappear, but is superimposed on the sharp image as a kind of gray veil or haze. Therefore, a substantial reduction in contrast is noticeable. However, the gain in quality compared with a simple radiograph is clearly visible in the example of the tomosynthetically acquired slice sequence of the knee in Fig. 16.2b [16.6, 7].

Due to the increased availability of electronic x-ray detectors, tomosynthesis systems are currently regaining scientific attention [16.8]. In modern systems, projection images are measured during movement and stored digitally using an image intensifier system. This allows subsequent image reconstruction that is superior to the analog blurring technique.

A related method, called *orthopantomography*, is now widely used in dental radiology. In this method, a panoramic view of rows of teeth is produced on an imaging plane that is curved to follow the jaw. However, sophisticated trajectories allow reconstruction of slices by geometric tomography as well. Nowadays, the term tomography, despite competitive modalities such as magnetic resonance imaging (MRI) or positron emission tomography (PET), is still most commonly associated with computed tomography (CT) or, more precisely, with x-ray CT.

16.2.2 Generations of CT Systems

Computed tomography avoids the superimposition of blurred planes and produces such high contrast that even soft tissue can be imaged well. The resulting leap in the quality of diagnostic imaging led to the enormous success of CT. Historically, four distinct generations of CT have emerged. Their classification relates to both the way in which x-ray tubes and detectors are constructed, and the way that they move around the patient. Figure 16.3a–d illustrates the different generations schematically.

First-Generation CT

The first generation of CT involves an x-ray tube that emits a single, needle-like x-ray beam, which is selected from the x-ray cone by means of an appropriate pinhole collimator. This geometry is referred to as *pencil beam*. A single detector is situated on the opposite side of the measuring field and the x-ray tube. The detector is moved synchronously along with the x-ray tube. This displacement is linear and is repeated for different projection angles γ (Fig. 16.3a). Depending on the specific attenuation properties of the tissue, the intensity of the x-ray is attenuated on its path through the body.

The amount of x-ray attenuation is measured by the detector and subsequently digitally recorded. For each angle γ, this step yields a simple, one-dimensional radiograph. However, from this initial radiograph, it is still not possible to determine the spatial distribution of the tissue attenuation coefficients. It is clear that, to determine the location of two consecutive objects on one projection line, the situation needs to be viewed sideways as well. This is the approach taken by CT, which views an object from all sides, since the projection angle is varied from 0° to 180°.

The first CT scanner, built by the company Electric and Musical Industries Ltd. (EMI), was based on this principle. In 1972, *Hounsfield* realized the scanner in the EMI central research laboratories [16.9]. For his invention, he jointly won the Nobel Prize for medicine together with Allen M. Cormack in 1979. The first ex-

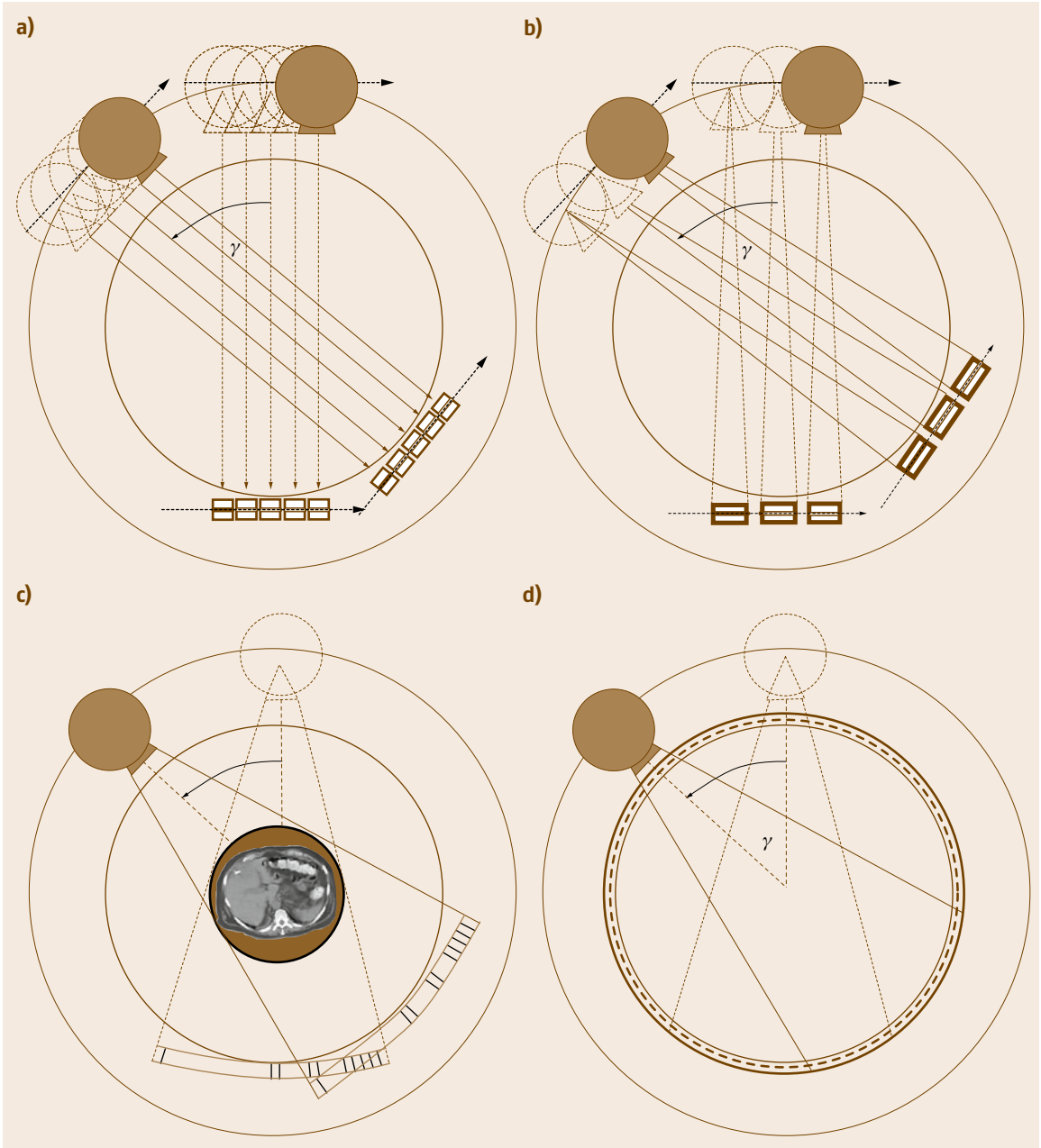

Fig. 16.3a–d First-generation CT devices are equipped with a pencil beam and a single detector. These are moved linearly, and the configuration is rotated through different projection angles **(a)**; CT scanners of the second generation have one x-ray source with fan-beam geometry, as well as a short detector array. The x-ray fan is created from a conical x-ray source by means of a slit-shaped collimator **(b)**; the third generation of CT scanners has a substantially larger angle of the x-ray fan and a longer detector array, such that the entire measuring field can be x-rayed simultaneously for one single projection angle **(c)**, and the fourth generation has a stationary closed detector ring **(d)**

periments by Hounsfield were performed in 1969 with a radioactive americium source that was linearly displaced along with the detector. Hounsfield collected data from 0° to 180° necessary for image reconstruction. The first reconstruction of a two-dimensional slice took 9 days – a clinically unacceptable processing time. However, for the first time, a two-dimensional slice image could be achieved that did not originate from averaging or blurring information, as in the conventional geometric tomography mentioned above. Figure 16.4 shows a very early EMI CT head scanner of 1972.

The first commercial scanners from EMI had a narrow focused x-ray beam and a single sodium iodide (NaI) scintillation detector. This pencil-beam principle, which is not practiced any more, is of fundamental importance as its mathematical methods for reconstruction can be understood most easily. Indeed, the mathematical methods of more modern geometries can be obtained from the pencil-beam geometry using suitable coordinate transformations. Figure 16.4a shows one of the first tomographs of the first generation produced by Siemens in 1972.

The subsequent rapid development of CT has been, and still is, driven by three essential goals: reduction of acquisition time, reduction of x-ray exposure, and, last but not least, reduction of cost. Throughout the course of optimizing these factors there are several historical stages, which are briefly described below.

Second-Generation CT

The computed tomograph of the second generation has an x-ray source with a narrow fan beam and a short detector array consisting of approximately 30 elements (Fig. 16.3b). However, since the aperture angle of the fan beam is small, the x-ray tube and detector array still need to be translated linearly before the projection angle is adjusted for another projection. In the earliest of the

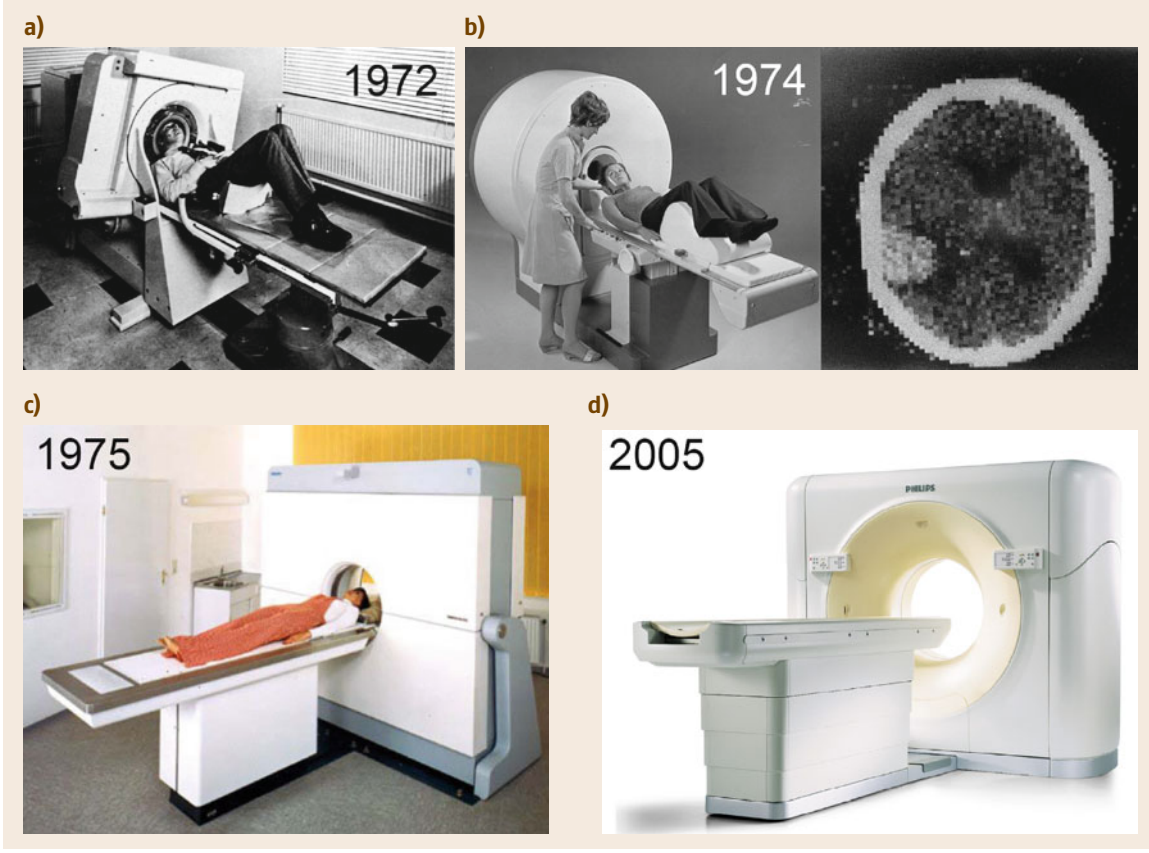

Fig. 16.4a–d Development steps of CT. **(a)** 1972: EMI head scanner (first generation); **(b)** 1974: Siemens Siretom (first generation); **(c)** 1975: Philips Tomoscan 200 (second generation); **(d)** 2005 Philips Brilliance (third generation)

second-generation scanners, the angle of the fan beam was about 10°.

Despite the need for linear displacement, the acquisition time was reduced to a few minutes per slice, as the detector array could measure several intensities simultaneously. However, the measuring field was still small. For this reason, and due to their long acquisition times, first- and second-generation scanners were mainly restricted to use in imaging the cranium. Figure 16.4b (right) gives an idea of the scale of the measuring field. The cranium can be fixed in the scanner and shows no large intrinsic movement during the acquisition time (relative to the spatial resolution that could be achieved at the time).

This is certainly not the case when imaging the area of the thorax or the abdomen, as the intrinsic movements of the heart and lung, as well as the movement of the diaphragm and soft organs of the abdomen, produce artifacts in the reconstructed images. The mathematical methods of reconstruction demand that all points of one slice are x-rayed from all angles from 0° through 180°. One object moving out of the imaging plane during rotation of the x-ray tube, due to patient movement, will inevitably result in errors in image reconstruction. Such image errors, referred to as motion artifacts, are described in detail in Sect. 16.4.4.

Third-Generation CT

The main goal of developments in the 1970s was to reduce acquisition time to less than 20 s. This was intended to give enough time to acquire an image of the abdomen with minimal error, while the patient held their breath. A major step toward achieving this goal was an extension of the second generation's fan-beam concept, i. e., the introduction of a substantially larger angle of the x-ray fan and a correspondingly longer detector array. Figure 16.3c shows a schematic illustration of this principle of third-generation scanners. Nowadays, the angle of an x-ray fan beam is typically between 40° and 60° and the detector array is usually constructed as an arc with between 400 and 1000 elements. In this way it is now possible to simultaneously x-ray the entire measuring field, which is currently wide enough to cover the torso, for each projection angle γ. As a result, the third generation of CT systems can completely abandon linear displacement of the x-ray tube.

The acquisition time for third-generation systems is reduced considerably, since continuous rotation can take place without interruption for linear displacement. The majority of CT scanners currently in use are fan-beam systems of the third generation. Figure 16.4c and d show two CT scanners of the second and third generation from 1975 and 2005, respectively.

Fourth-Generation CT

The fourth generation of CT scanners does not differ from the third generation with respect to the x-ray tube. The fan-beam source also rotates continuously around the measuring field without any linear displacement. The difference is in the closed, stationary detector ring with up to 5000 single elements. The x-ray tube rotates either outside (Fig. 16.3d) or inside the detector ring.

If the x-ray tube is outside the detector ring, it is necessary to prevent the x-rays from radiating through the detectors from behind. Therefore, the detector ring is dynamically tilted away from the path of the tube. In this way, the line of sight between the tube and the appropriate section of the detector ring only passes through the patient (and patient table) and not through the electronics behind the detectors.

Fourth-generation tomographs establish *inverse fans*, which are centered on detectors rather than on the x-ray focus. An inverse fan is also referred to as a *detector fan*. An inverse fan can be very dense, limited only by the sampling rate at which individual detectors can be read out. As a result, unlike third-generation tomographs, this scanner is not limited to the spatial resolution of a single fan beam.

16.2.3 Spiral CT

Another development, which was a great leap forward in capability from that of the third generation, led to what is identified by *Bushberg* et al. [16.10] as the sixth generation of tomography scanners. This refers to the introduction of slip-ring technology, which enables spiral or helical sampling.

As the x-ray tube must be continuously supplied with energy, the rate of circular movement was previously limited by the attachment of an electric cable, which was mounted on a spool. In this process the cable was unwound in one direction and carefully wound up in the other. This represented a huge obstacle to the reduction of acquisition time. The x-ray sampling unit had to stop and start again after a certain angle of rotation.

Although data could be collected throughout both clockwise and counterclockwise rotations, limits were placed on high velocities due to the increasing torsional moment. This problem was solved by the introduction of slip-ring technology. In this technology, the energy is provided via sliding contacts situated between the outside of the sampling unit, in what is called the *gantry*,

and the rotating sampling unit. This enables the sampling unit carrying the x-ray source and, in the case of third-generation scanners, the detector array to rotate continuously. As a result of slip-ring technology, rotation frequencies of two rotations per second, i.e., *subsecond scanners*, are nowadays commonplace.

However, there are also smaller, more compact devices, in which the sampling unit is independent from an external energy supply during rotation, making use of accumulators. An example is given by the mobile Philips Tomoscan M CT scanner, where accumulators are mounted on the rotating sampling disk and a capacitive radiofrequency (RF) link is used for data transfer.

The slip-ring innovation enabled a new acquisition technique. Along with a continuous motion of the patient table through the sampling unit, it became possible to measure data in the shape of a spiral (strictly speaking, the x-ray tube trajectory is a helix). The spiral CT technique was demonstrated successfully using a prototype by *Kalender* in 1989 [16.11]. The spiral CT technique is discussed in more detail in Sect. 16.4.3.

16.3 Computed Tomography Technology

Computed tomography systems consist of a *front-end*, i.e., the scanner unit, and a *back-end*, i.e., the control console and viewing station. All components of the front-end, i. e., the x-ray tube, x-ray filter, aperture unit, collimator, detector system, high-voltage generator, cooling system, data-acquisition system (DAS), slip ring, patient table, motors, motor controllers, as well as mechanical components, are highly developed today. However, due to their key position in the system, only two main components of the front-end will be discussed here: the x-ray tube and the corresponding detector system. For a detailed discussion of the physics of x-ray generation, photon–matter interaction, x-ray detection, and photon statistics the reader is referred to [16.4].

16.3.1 X-Ray Generation

X-ray radiation is of electromagnetic nature; it is a natural part of the electromagnetic spectrum, with a range that includes radio waves, radar and microwaves, infrared, visible and ultraviolet light, to x- and γ-rays. In electron-impact x-ray sources, the radiation is generated by deceleration of fast electrons entering a solid metal anode and consists of waves with a range of wavelengths roughly between 10^{-8} and 10^{-13} m. Thus, the radiation energy depends on the electron velocity v, which in turn depends on the acceleration voltage U_a between the cathode and anode. In medical diagnostics, acceleration voltages are chosen between 90 and 140 kV, for radiation therapy they lie between 10 and 300 kV, and for material testing they can reach up to 500 kV.

Electrons are emitted from a filament, which is directly heated to approximately 2400 K to overcome the binding energy of the electrons to the metal of the filament. Filaments are usually made of thoriated tungsten with a melting point of 3683 K. Due to their thermal energy, electrons are boiled off from the filament. This process is called thermionic emission. To produce a small electron focus on the anode, the trajectories of the accelerated electrons must be controlled by electron optics. The focusing device is a cup-shaped electrode (frequently named a Wehnelt cylinder) that forms the electric field near the filaments such that the electron current is directed to a small spot on the anode.

While the acceleration voltage determines the energy interval of the x-ray spectrum, the intensity of the generated x-ray spectrum or the number of x-ray quanta is solely controlled by the anode current. The acceleration voltage and the anode current can be controlled by the user.

With the entry of accelerated electrons into the anode, sometimes also called the *anticathode*, several processes take place close to the anode surface. Generally, the electrons are diffracted and slowed down by the Coulomb fields of the atoms in the anode material. The deceleration results from the interaction with the orbital electrons and the atomic nucleus. As known from classical electrodynamics, acceleration and deceleration of charged particles creates an electric dipole, and electromagnetic waves are radiated. Usually, several photons emerge throughout the complete deceleration process of one single electron. It can happen, however, that the entire energy eU_a of an electron is transformed into a single photon. This limit defines the maximum energy of the x-ray radiation.

Due to the fact that the slowing down of electrons in the anode material is a multiprocess deceleration cascade, a continuous distribution of energies is produced, the so-called *bremsstrahlung*. Since the free electrons

are unbound, their energy cannot be quantized. The continuous *bremsstrahlung* is superimposed by a characteristic line spectrum, which originates from direct interaction of fast electrons with the inner shell electrons of the anode material. If an electron on the K-shell or K-orbital is kicked out of the atom by a collision with a fast electron, i. e., the atom is ionized by the loss of an inner electron, an electron of one of the higher shells fills the vacant position on the K-shell. As the inner shells represent states having lower potential energy than the outer shells, this process is accompanied by the emission of a photon. This process creates sharp lines in the x-ray spectrum that are characteristic fingerprints for the anode material.

It should be noted at this point that the image quality of CT specifically suffers from the fact that x-ray attenuation is a complicated function of wavelength. The details of the functional behavior are given in the next section. Generally, one has to bear in mind that a low-energy x-ray, i. e., radiation with a longer wavelength, is more strongly attenuated when passing through matter than high-energy x-ray. (Low-energy quanta are generally undesired in x-ray imaging. They increase the dose to the patient, but do not contribute to imaging, because they are almost totally absorbed by the human body.) As a consequence, the center of the polychromatic x-ray is shifted to higher energies (harder radiation). This is the origin of what is called beam hardening, which produces artifacts in the reconstructed images.

Generally, a flat metal filter measuring a few millimeters is mounted onto the x-ray tube. The filtering of the useful beam reduces the number of x-ray quanta while increasing the average energy of the radiation. This prehardening of the radiation reduces beam-hardening artifacts during image reconstruction and the dose to which the patient is exposed.

Unfortunately, the quantum efficiency of the conversion from kinetic energy into x-ray radiation, for a tungsten anode (W, $Z = 74$) working with an acceleration voltage of $U_a = 140\,\mathrm{kV}$, is roughly on the order of $\eta = 0.01$. This means that 99% of the kinetic energy is transferred locally to the lattice, heating up the anode. As a result, CT x-ray tubes have serious heating problems.

Since it is the energy deposition in the target volume that produces the heat load, the tube current and the duration of exposure, or more precisely the product of current in milliamperes and exposure time in seconds, are two important parameters of the practical scan protocol that the radiologist has to choose appropriately. The heat capacity of an x-ray tube is measured in *heat units*. Therefore, for several decades, rotating anode disks have been used to distribute the thermal load over the entire anode. The anode target material is rotated about the central axis, and therefore new, cooler anode material is constantly rotated into position at the focal spot [16.12]. In this way, the energy of the electron beam is spread out over a line, called the focal line, rather than being concentrated at one single point. In Fig. 16.5a–c a modern Philips MRC 600 x-ray tube is shown. A liquid-metal-filled spiral-groove bearing allows very high continuous power compared with conventional ball bearings. Often, a heat exchanger is placed on the rotating acquisition disk to cool the anode.

Ideally, x-rays should be created from a point source, because an increase in source size will result in a penumbra fringe in the image of any object point. The size and shape of the x-ray focus seen by the detector determines the quality of the resulting image. The effective target area, called the optical focus, depends on the orientation of the anode surface that is angulated with respect to the electron beam. The projection of the focus shape onto the detector must be minimized to obtain a sharp image. However, this surface angle increases the tube power limit, because it allows the heat to be deposited across a relatively large spot while the apparent spot size at the detector will be smaller by a factor of the sine of the anode angle [16.12]. The image quality is degraded by a large focus diameter, due to significant partial shadow areas of each object point. The mathematical expression that measures the image quality is called the *modulation transfer function* (MTF). A large angle between the incident electron beam and the anode surface normal is generally not desired, because there is a certain probability that the electrons will be elastically reflected from the surface and thus not contribute to x-ray generation. The probability of this backscattering effect increases as the atomic number of the anode material increases and as the angle between the surface normal and the anode rotation axis decreases.

Typically, the x-ray focus diameter for diagnostic tubes is found to be between 0.3 and 2 mm. The penetration depth of electrons into the anode depends on the kinetic energy and the anode material and can be found to be up to 30 μm. The radiologist may have the option of choosing between two focus sizes. This is technically realized by focusing the electron beam onto two target points with different anode orientations. In some systems the spatial resolution of the detector can also be doubled by switching between two foci during data acquisition. This concept is called a flying focus.

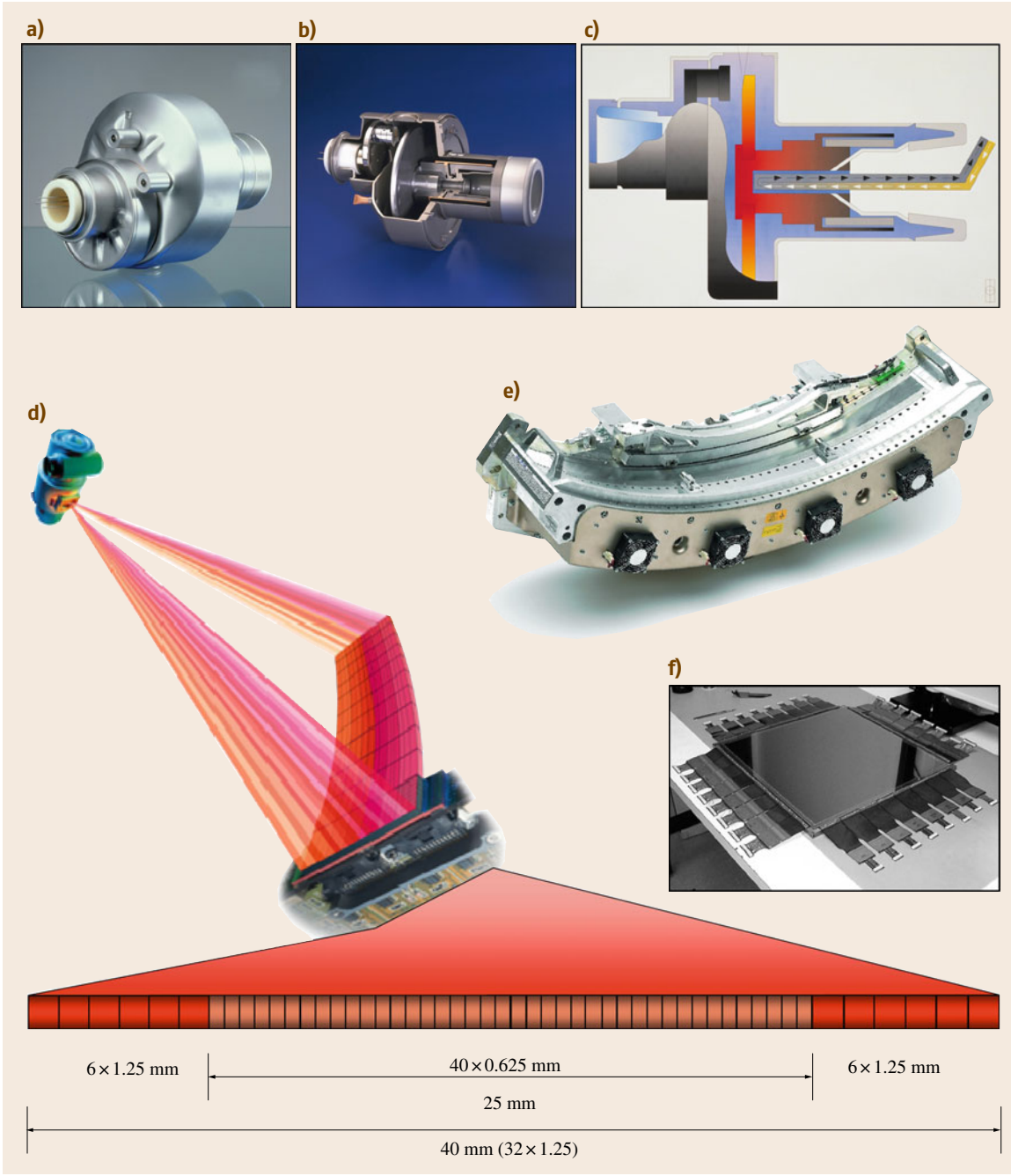

Fig. 16.5a–f Modern high-power x-ray tube (**a**,**b**) and schematic illustration of a modern x-ray tube with a rotating anode disk (**c**), schematic illustration of a multislice detector (**d**), a detector unit of a 64-row CT system (**e**), and the realization of a $41 \times 41\ \mathrm{cm}^2$ flat-panel detector with 2048×2048 pixels (**f**)

A second effect that influences imaging quality is caused by the anode surface. X-ray beams leaving the anode tangentially to the anode surface are reduced in intensity when arriving at the detector. This intensity reduction is due to the self-absorption of photons by the anode, caused by the microscopic roughness of the anode surface. The x-ray intensity decreases gradually with a reduction in the angle between beam and anode surface. This effect, which is called the *heel* effect, grows during the lifetime of any x-ray tube, because the roughness of the anode surface increases due to erosion by electron bombardment along the focus line. In modern CT systems the cone of the utilized x-rays is becoming larger and larger. Therefore, it is important to know the radiation characteristics of the anode, because the basic assumption of the imaging principles of fluoroscopy and of CT reconstruction is that the object to be scanned is illuminated homogeneously. Slight deviations from a homogeneous beam profile can be compensated for by specially formed filters mounted on the x-ray tube and by detector calibration.

16.3.2 Detector Systems

Typically, x-ray quanta are not measured directly, but are detected via their interaction products (for example, emitted photoelectrons). The overall detection efficiency is primarily determined by the geometric efficiency (also called the *fill factor*) and the quantum efficiency (also called the *capture efficiency*). The geometric efficiency refers to the x-ray-sensitive area of the detector as a fraction of the total exposed area, and the quantum efficiency refers to the fraction of incident quanta that are absorbed and contribute to the signal. The overall detection efficiency is the product of the geometric and the quantum efficiencies.

Gas Detectors

X-ray radiation is able to ionize gases. This fact was discovered very early in the last century and led to the development of the well-known Geiger–Müller counter. In the first tomographic experiments carried out by Cormack and Hounsfield, the Geiger–Müller counter was used as a detector in pencil-beam geometry. In the early days of clinical CT, gas-based detector arrays were also manufactured for what are known as third-generation scanners in fan-beam geometry. Even today, some scanners using high-pressure xenon are in use. The photoelectric interaction, $h\nu + \mathrm{Xe} \rightarrow \mathrm{Xe}^{+} + \mathrm{e}^{-}$, describes the first part of the detection process chain. Xenon ions and electrons are attracted by high voltage to a cathode and an anode, respectively. A series of alternating cathode and anode pairs forms the detector array [16.4]. The current produced by recombination is a measure of the x-ray intensity entering the detector.

A weak quantum efficiency (a low probability for photoelectric absorption) can be compensated for by high-pressure and tall ionization chambers. Another advantage of tall chambers is improved directional selectivity of the detector element. Since the ionization probability is proportional to the travel length of x-ray quanta inside an element (one cathode–anode block), detection of x-ray quanta with an oblique entrance will be suppressed. In this way, a tall detector element has built-in collimation. However, the septa between detector elements are insensitive regions that will decrease the geometric efficiency of the detector.

Scintillation Detectors

Today, almost all modern CT systems are equipped with scintillator detectors. Such a detector essentially consists of two main components: a scintillator medium and a photon detector. In a first step, the short-wave x-ray radiation entering the detector is converted into long-wave radiation (light) inside the scintillation material. Typical scintillator materials used are cesium iodide (CsI), bismuth germanate (BGO), and cadmium tungstate ($CdWO_4$). The choice of material is critical and depends on the desired quantum efficiency for the conversion from x-ray to light and on the time constant for the conversion process, which determines the *afterglow* of the detector. For very fast fluorescence decay, i. e., a very small time constant, as required by modern subsecond scanners, ceramic materials made of rare-earth oxides such as gadolinium oxysulfide (Gd_2O_2S) are used.

On the rotating sampling unit, the series of detector elements is arranged in a circle segment with the x-ray source at its center. In Fig. 16.3c this is schematically shown for a third-generation scanner. X-rays that have been scattered may undergo deflection through a small angle and finally reach the detector. This detection is undesired because it reduces the contrast of the image. To suppress the measurement of scattered x-ray quanta, collimator lamella are attached to each element. Such an antiscatter collimator grid is directed toward the x-ray focus to filter out photons not traveling in the line of sight between the x-ray source and the detector. Without an antiscatter grid, the image quality would be significantly reduced.

However, there is an obvious disadvantage of the antiscatter grid. To block an oblique entrance of scat-

tered x-ray photons effectively, a minimum lamella thickness of 0.1 mm is required. In practice, the detector elements have a total geometric efficiency of about 50–80% [16.13]. This decreased fill factor leads to an undesired reduction in spatial detector resolution.

Solid-State Multislice Detectors

Crystal- and ceramic-based solid-state detectors described in the previous section can be extended to multirow or multislice detector systems. The key feature of such multirow arrays is a maximum effective x-ray-sensitive area. This feature is quantified by the fill factor, which is explained below. Xenon high-pressure gas detector array systems cannot be easily extended to flat area detector systems. Therefore, all modern multislice CT systems are based on solid-state scintillation detectors.

In Fig. 16.5d, a cone-beam detector system is shown schematically. In contrast to detector systems in technical CT systems, for example, in micro-CT (where flat-panel detectors are employed), almost all clinical CT systems are equipped with cylindrical detector units. As illustrated in Fig. 16.5d, the multiarray system forms a cylindrical barrel with the x-ray source as its center. If the number of rows of such multislice detector systems is chosen to be very high, the orientation of the respective x-ray fan inside the cone beam, relative to the axial slice, becomes significant, and the requirements of image reconstruction increase. However, modern CT systems are equipped with cone-beam sampling units due to improved spatial resolution and faster image acquisition. Image reconstruction in cone-beam systems is discussed in Sect. 16.4.

Different technical configurations of multislice detector systems are available today. Usually, detector units can be partitioned and combined. This flexibility is achieved by the electronic interconnection of pairs of detector segments leading to a desired slice thickness.

Solid-State Flat-Panel Detectors

Without reconstruction mathematics that are adapted to the cone-beam situation, image artifacts arise for higher x-ray fan angulations, even in a 16-row detector system. This leads to clinically unacceptable image quality. In any case, the reconstruction algorithms used for the cone-beam geometry need to be revised for practical implementation. Therefore, a logical step forward is to leave multirow detector arrays and move in the direction of real flat-panel detector systems, which have recently become commercially available. However, they were not originally designed for use in CT systems, but rather to compete with established radiography systems using film cassettes, computed radiography cassettes, and image intensifiers.

Each sensor element of a flat-panel detector consists of a photodiode and a thin-film transistor (TFT). Both are made of amorphous silicon on a single glass substrate. The pixel matrix is coated with an x-ray-sensitive layer. Multichip modules are used as readout electronics at the edge of the detector field. The x-ray-sensitive coating is, for instance, a cesium iodide layer. The basis is the single glass substrate with a silicon matrix of 2048×2048 sensors, each $200\,\mu m$ in size. The monolithic structuring is done with thin-film technology such that a composition of a set of medium-sized subpanels, which have undesired dead zones at the interfaces, potentially producing imaging artifacts, is not required. A final cesium iodide (CsI) coating forms the scintillator layer of the detector.

The CsI layer is applied directly onto the pixel matrix by a physical deposition process. The production technique is known from semiconductor production. Physical and chemical processing steps, i. e., the combination of photolithography and further etching phases, are applied to produce the finely structured detector elements. This leads to an x-ray-sensitive detector field with a desired high fill factor, i. e., the ratio of the *x-ray-sensitive area of the detector* to the *total area of the detector*.

X-ray quanta entering the detector are converted into visible light in the upper CsI scintillator layer. The light photons are guided to the photodiodes of the next processing layer. The photons are absorbed, thereby producing an electric charge in the photodiodes that is proportional to the intensity of the x-ray radiation.

During detector exposure, the electric charge is integrated and stored in the detection element, which acts as a capacitor. The actual readout process is initialized by the thin-film transistor, which switches the charge to the readout electronics via a data link. There, amplification and analog-to-digital conversion are performed on the same chip, resulting in fast operation with low noise. In Fig. 16.5f, a preassembly, raw detector with ribbon-cable data links [16.14] is shown. Its 4 194 304 pixels are integrated onto a $41 \times 41\,cm^2$ active area.

A highly desired system property of the digital scintillation detector system is linear dynamics over a wide range of illumination. In this way, high- and low-dose applications have the same contrast information, i. e., excellent contrast resolution. Film systems are capable of imaging objects with high contrast within a very narrow exposure range only. If the object is over- or

underexposed, the contrast of the image can easily be too low. Due to the linear response characteristic curve of the digital system, it is robust against over- and underexposure. However, within the range of low-contrast imaging, flat-panel systems do not achieve the quality of the dedicated CT detector systems described in the sections above [16.13].

In addition to a linear detector dynamics characteristic, another important advantage of the flat-panel detector is its excellent spatial resolution. To optimize the spatial resolution, CsI is evaporated onto the matrix so that direct contact between the scintillation material and the carrying photodiode matrix is established. This manufacturing step is designed in such a way that CsI grows anisotropically, forming needles on the matrix. If x-ray quanta are converted into visible light inside the CsI structure, the emerging photons are, in all likelihood, traveling along the needles, because they act as a fiber-optic cable. In this way, photons are guided directly onto the photodiode or in the opposite direction.

The photons that are traveling in the opposite direction face a mirror on the top side of the CsI layer that ensures that eventually almost all photons find their way to the photodiode. This light guidance effect of the CsI fiber structure is the reason for the high quantum efficiency of digital flat-panel detectors. The x-ray-sensitive CsI coating can be made very thick to obtain high quantum efficiency and also to suppress broad photon scattering, which would reduce the spatial resolution. The scintillation light is bundled by the CsI fibers onto a small point on the photodiode matrix. However, an isotropic CsI layer must always find a compromise between high quantum efficiency and high spatial resolution. Figure 16.12b in Sect. 16.7 shows a a prototype volume or cone-beam CT equipped with a flat-panel detector.

16.4 Image Reconstruction

The fundamental problem of computed tomography can be easily described: Reconstruct an object from its shadows or, more precisely, from its projections. An x-ray source with a fan- or cone-beam geometry penetrates the object to be examined, such as a patient in medical applications, a skull found in archeology, or a specimen in nondestructive testing (NDT). In so-called third-generation scanners, the fan-shaped x-ray beam fully covers a slice section of the object to be examined. Depending on the particular paths, the x-rays are attenuated to varying extents when passing through the object; the local absorption is measured with a detector array.

Of course, the shadow that is cast in only one direction is not an adequate basis for determination of the spatial distribution of distinct structures inside a three-dimensional object. To determine this structure, it is necessary to irradiate the object from all directions. Let $p_{\gamma_i}(\xi)$ represent the attenuation profile of the beam as a function of the x-ray detector array coordinate ξ under a particular projection angle γ_i. If the different attenuation or absorption profiles are plotted over all angles of rotation γ_i of the sampling unit, a sinusoidal arrangement of the attenuation or projection integral values is obtained. In two dimensions, these data $p_{\gamma_i}(\xi)$ represent the Radon space of the object, which is essentially the set of raw data. From a mathematical point of view, image reconstruction in computed tomography is the task of computing the spatial structure of an object from the shadows that it casts. The solution to this problem is complex and involves techniques from physics, mathematics, and computer science. The described scenario is referred to as the inverse problem in mathematics.

In computed tomography, the meaning of the mathematical term *inverse problem* is immediately apparent. The spatial distribution of attenuating objects that produce the projection shadow is not known a priori. This, actually, is the reason for acquiring the projections along the rotating detector coordinate ξ over a projection angle interval of at least 180°. It is an inversion of integral transforms. From a sequence of measured projection shadows $\{p_{\gamma_1}(\xi), p_{\gamma_2}(\xi), p_{\gamma_3}(\xi), \ldots\}$, the spatial distribution of the objects, or more precisely the spatial distribution of the attenuation coefficients $\mu(\xi, \eta)$ within a chosen section through the patient, must be estimated.

In 1961, the solution to this problem was applied for the first time to a sequence of x-ray projections by which an anatomical object had been measured from different directions. Allen MacLeod Cormack (1924–1998) and Sir Godfrey Hounsfield (1919–2004) were pioneers of medical computed tomography and in 1979 received the Nobel Prize for medicine for their epochal work during the 1960s and 1970s.

16.4.1 Fourier-Slice Theorem

Depending on the path η which the x-ray quanta take through the body – starting at the x-ray tube $\eta = 0$ and

Fig. 16.6a–g From the raw data to the reconstructed image. Sinogram of attenuation or projection values **(a)**, high-pass-filtered projection values **(b)**, backprojection of the filtered projection **(c)**, accumulation of all backprojections of the high-pass-filtered **(d)** and the native **(e)** projection profiles; data acquisition of spiral CT **(f)**, row-data interpolation for spiral CT **(g)** ▶

ending at the detector $\eta = s$ – the intensity of the rays will be attenuated differently. After taking the logarithm of the intensity measured on detector element ξ the sum of attenuation values $p_\gamma(\xi)$ is obtained along the x-ray path for the projection angle γ.

The x-ray source rotates around the object to be examined, penetrating it with x-rays. The sum of attenuation values, the so-called projection integral $p_\gamma(\xi)$, is measured and saved for each angle. Therefore, the projection integral – plotted over all angles – takes a sinusoidal course (Fig. 16.6a). This plot that collects the raw data of the measurement is called a sinogram and represents the Radon space of the object, named after the Austrian mathematician *Radon* [16.15].

The key theorem that describes the relation between the Fourier transform of the projection integral and the Fourier transform of the desired image is the Fourier-slice theorem. One is interested in the spatial distribution of attenuation values $f(x, y) = \mu(\xi, \eta)$ having measured only the projection data $p_\gamma(\xi)$.

The Fourier-slice theorem ensures that the one-dimensional Fourier transform $P_\gamma(q)$ of the measure projection integral $p_\gamma(\xi)$ can be identified with a radial line in the Cartesian Fourier space $F(u, v)$ of the object $f(x, y)$ drawn at the angle γ of the corresponding measurement, with $u = q\cos\gamma$ and $v = q\sin\gamma$. Filling the Fourier space in that way over all angles γ leads to a complete Fourier representation of the object, which can be reconstructed in principle by an inverse two-dimensional Fourier transform. For a detailed discussion the reader is referred to [16.4].

16.4.2 Filtered Backprojection

The Fourier-slice theorem is not directly implemented due to some interpolation problems that would arise. In today's CT systems, so-called filtered backprojection is widely used. Within this method, which is also called the convolution method, the projection integral data $p_\gamma(\xi)$ are digitally filtered. Figure 16.6a,b shows how this is done in the frequency domain. The linear weighting $|q|$ of the Fourier-transformed projection profile $P_\gamma(q)$ is essentially a high-pass filter. Consequently, the filtered projection profile $h_\gamma(\xi)$ shows the changes along the profile only. The result of the high-pass filtering of the measured attenuation profile $p_\gamma(\xi)$ is illustrated in Fig. 16.6b. It can be seen that the sinusoidal structure of the data is preserved. However, due to the high-pass filtering, only changes of $p_\gamma(\xi)$ are represented by $h_\gamma(\xi)$.

This filtered profile $h_\gamma(\xi)$ is projected back in the direction γ of the measurement of $p_\gamma(\xi)$. In Fig. 16.6c this is exemplarily demonstrated for a single backprojection angle γ. Obviously, a single filtered backprojection alone does not represent the image of the object. However, the errors of one direction are consistently compensated by accumulation of the backprojections of all available views in the interval $\gamma = [0, \pi)$.

The concept for reconstruction of the tomographic image $f(x, y)$ from the projection values $p_\gamma(\xi)$ is demonstrated by a successive backprojection. In Fig. 16.6d the intermediate results of the reconstruction process of a tomographic abdomen image are shown for an increasing number of projection angles $N_\mathrm{p} = \{1, 2, 3, 10, 45, 180\}$. This sequence reveals that a sufficiently high number of projection angles is needed to reconstruct the image of the object. In Fig. 16.6e the intermediate results of the simple backprojection, i. e., the direct backprojection of the measured projection integral $p_\gamma(\xi)$, is shown. This naive strategy leads to a blurred image independent of the number of backprojection angles.

When CT images are compared, it is important to know the exact weighting function within the filtered backprojection. The linear weighting with $|q|$ as described above is the mathematically ideal case. In practice, the filter is often less progressive in the high-frequency domain. The actual type of weighting can be chosen at the console of the scanner. The operator is asked to choose a filter kernel from a filter bank including a variety of gradually changing weightings from *very sharp* to *very smooth*. The optimal choice of a filter kernel is always a compromise between a high noise level with fine spatial resolution and smooth images with low spatial resolution [16.4].

16.4.3 Raw-Data Interpolation for Spiral CT

A first step toward a true volume image is the so-called spiral CT method (Sect. 16.2.3), which was proposed by

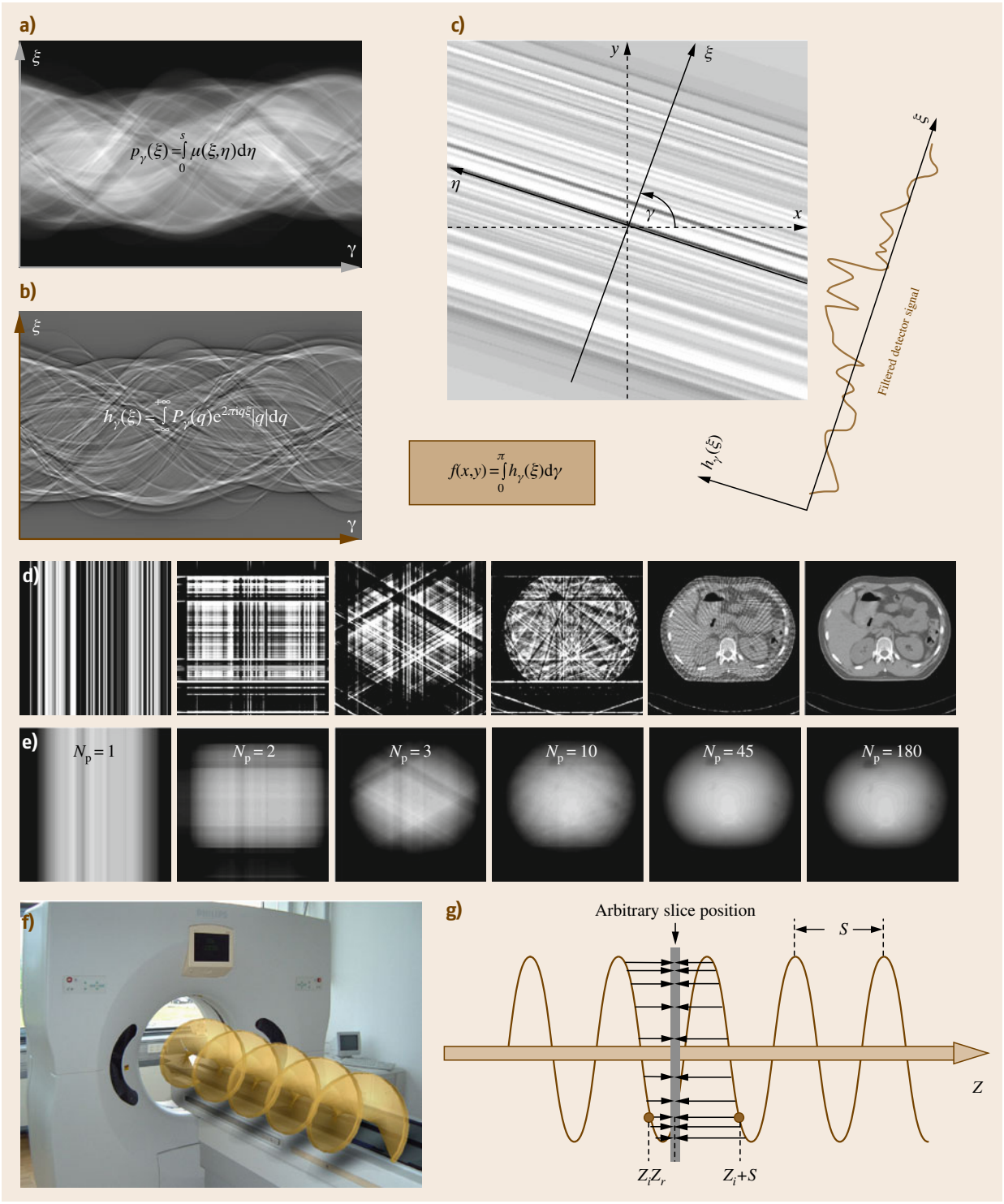
a)
ξ
$p_\gamma(\xi)=\int_0^s \mu(\xi,\eta)\mathrm{d}\eta$
γ
b)
ξ
$h_\gamma(\xi)=\int_{-\infty}^{+\infty} P_\gamma(q)e^{2\pi iq\xi}|q|\mathrm{d}q$
γ
c)
y
ξ
η
γ
x
$f(x,y)=\int_0^\pi h_\gamma(\xi)\mathrm{d}\gamma$
Filtered detector signal
$h_\gamma(\xi)$
d)
e)
$N_p=1$
$N_p=2$
$N_p=3$
$N_p=10$
$N_p=45$
$N_p=180$
f)
g)
Arbitrary slice position
S
Z
Z_iZ_r
Z_i+S

Kalender in 1989 at the annual Radiological Society of North America (RSNA) conference [16.11].

The inadequacies of the simple slice stack produced by conventional CT are easy to understand. Due to the preset collimation, each slice has a certain width, which is also referred to as the slice thickness. Within this slice thickness the intensity is weighted with its sensitivity profile – given by the source intensity distribution inside the collimation and the detector sensitivity profile – and then averaged.

This averaging process is a problem in all cases in which the object is characterized by boundaries which are angulated with respect to the axial slice, i. e., where structures to be displayed quickly change in the direction of the table feed. In these cases, the averaging process results in a step-like slice stack so that the structure to be displayed has a staircase-like appearance. The development of slip-ring technology, which has already been briefly discussed in Sect. 16.2.3, made it possible to rotate the sampling unit, i. e., the tube and detector array system, continuously. If the table feed is kept constant during the rotation, then the x-ray source rotates around the patient on a spiral path; strictly speaking, this movement describes a helical trajectory (Fig. 16.6f).

This orbit interpretation is based on a coordinate system attached to the patient table, since the x-ray source does of course still run along a circular path. The spiral path only arises from the patient's view. With this concept, complete projection data acquisition of an object is possible, and the scan time for a volume could be considerably reduced in comparison with conventional tomography.

Indeed, it is remarkable that spiral CT technology works at all. An essential requirement for the reconstruction methods described in Sects. 16.4.1 and 16.4.2 is the completeness of the raw data. This means that an object in the measurement field can only be reconstructed if all points of the object are illuminated from all sides, i. e., over 180°. This condition is the reason why artifact-free conventional CT scans of the heart are practically impossible because the heart motion shifts parts out of the slice to be reconstructed while the sampling unit rotates around the heart.

Thus, the projection data to be used for the reconstruction process do not fulfill the consistency condition. Rather, the differences between the projection data of a complete cycle should only be caused by the change of perspective. The reconstructed tomogram is thus impaired by motion artifacts, which will be described in detail in Sect. 16.4.4.

In spiral CT scanners, the motion of the objects to be reconstructed is in fact the decisive innovation compared with conventional CT scanners. The object to be examined is no longer scanned in a single plane. The reason for this is that, due to the continuous patient table feed, the source trajectory is not a closed circular orbit. Therefore, a complete set of raw data is not available for the reconstruction process – the data are inconsistent in terms of Sect. 16.4.1.

The key idea governing the reconstruction process of the spiral CT method is based on the assumption that the missing data of one slice can be completed by interpolation (Fig. 16.6g). If this has been done, then the two-dimensional reconstruction procedures described in Sect. 16.4.2 are again available without any restriction. Figure 16.6g shows the simplest principle of a slice interpolation. The helical rise, i. e., the path along which the table is moving during one 360° rotation of the sampling unit, will be denoted with s here.

One may now select an arbitrary slice position z_r because no preferred axial position regarding the data basis exists due to the constant table feed. For the selected slice there initially is only a single projection angle γ_r for which the projection dataset $p_{\gamma_r}(\xi)$ is available. The projection data $p_\gamma(\xi)$ of all other projection angles must be provided accordingly by means of interpolation. For this purpose, the data that have not been measured under the other required projection angles in the selected slice position z_r must be interpolated on the basis of the closest neighboring angles of the helical trajectory that have actually been measured. Contrary to conventional CT, one has to consider the table speed v as a function of the rotation frequency $1/T_{rot}$ of the sampling unit. This yields the table feed per rotation or the helical rise $s = v/T_{rot}$. If one includes the width or thickness of the x-ray fan d defined by the collimator, then these parameters are usually combined to define the new scan protocol parameter pitch $p = s/d$.

16.4.4 Artifacts

Artifacts are image errors that may emerge due to a variety of reasons. Artifacts can originate from a simplification of the reconstruction method – to date usually the filtered backprojection – which assumes monochromatic radiation or continuous representation of the projection signal. Artifacts may also stem from the use of special sampling technologies and detector arrangements, or simply from defective detector elements. Corrective actions may only be taken if the causes of such artifacts are known. Such countermeasures are in

fact very important, since the filtered backprojection has the disadvantage that artifacts are projected back over the entire image so that the overall diagnostic value of the image is reduced or completely destroyed. In this section a brief overview of CT artifacts is given [16.4].

Partial-Volume Artifacts

If a detail of an object consists of a sharply contrasted boundary, the limited resolution of a detector system of course becomes particularly noticeable. The boundary will usually not be located directly at the edge between one detector element and another. Therefore, the x-ray intensity at the corresponding element that has to image this boundary will be linearly averaged over the detector width $\Delta\xi$. Due to this averaging step, the object is blurred. Due to the superposition of filtered backprojections from all directions, this inconsistency leads to artifacts within the reconstructed image which are visible as streaks from the origin of the inconsistency along the backprojection path. Partial-volume artifacts are thus observed, for instance, as ghost lines that extend, particularly, from straight object boundaries. This is due to the fact that the backprojections from the other directions are not able to consistently correct an erroneously detected value, which has been projected back over the entire image. As a countermeasure, the beam may be collimated finely and the corresponding artifacts will be reduced.

Beam-Hardening Artifacts

X-rays produced by electron-impact sources, where fast electrons are entering a solid metal anode, cannot be monoenergetic or monochromatic. In Sect. 16.3.1, the different spectral x-ray components have been introduced, such as the continuous spectrum of the bremsstrahlung (from fast electrons decelerated by the Coulomb fields of the atoms in the anode material) and the characteristic emission lines. Radiation attenuation does not only depend on the path length but is also a function of the specific, wavelength-dependent interaction between x-rays and the material concerned. The reconstruction is in this case – similar to the partial-volume artifact described above – impaired by the nonlinearities which occur here. The beam-hardening artifact is caused by the nonlinear relation between the attenuation values μ and the measured values of the projection p. If an x-ray beam with broadband energy spectrum passes through an object, the spectrum changes along the path. This is due to the fact that different bands of the frequency spectrum are differently attenuated, depending on the specific attenuation coefficients $\mu = \mu(\xi, \eta, E)$ of the material being radiographed. In general, low-energy, i. e., soft, x-ray beams, are more strongly absorbed than high-energy, hard x-ray beams. This is the reason why this effect is named hardening of the x-ray spectrum and the corresponding image error is named the beam-hardening artifact. Similar to the partial-volume artifact, the beam-hardening artifact can be explained by the inconsistency of the individual projection values from different directions, which cannot complement each other correctly within the filtered backprojection method. One corrective method applied in virtually all CT scanners consists of filtering the soft radiation next to the source, i. e., before the radiation reaches the tissue. This may, for example, be done with thin aluminum or copper foils, and for a single material with known properties, it is of course possible to correct for beam hardening computationally.

Metal Artifacts

One known problem in CT is the appearance of metal artifacts in reconstructed CT images. Low-energy x-rays are attenuated more strongly than high-energy x-rays. Recall that the absorption is given by $\alpha \propto Z^4\lambda^3$. Due to the Z^4 dependence, this beam-hardening effect is prominent for metals that are introduced into the human body, such as dental fillings or hip prostheses, and leads to inconsistencies in the Radon or projection space. These inconsistencies observed in the integral attenuation values are due to the polychromatic x-ray spectrum produced by the x-ray tube. Additionally, without applying the dual-energy principle, the total attenuation of the x-ray intensity is an a priori unknown combination of the photoelectric effect and the Compton effect. This often leads to artifacts in the reconstructed images in the form of dark stripes between metal objects with light, pin-striped lines covering the surrounding tissue. Besides beam hardening, another origin of metal artifacts is a higher ratio of scattered radiation to primary radiation, causing a low signal-to-noise ratio (SNR) in the metal shadow. This effect will be discussed in the next section. However, inconsistent projection data can also be repaired with surrogate data created by interpolation or be treated as missing data in order to ignore the inconsistent data in a statistical approach. The problem with interpolated surrogate data is that they always include residual inconsistencies due to missing information during interpolation. On the other hand, within the missing data approach, a brute-force method is applied to eliminate inconsistencies. However, the problem with this strategy is that the reconstruction

actually suffers from voids in the projection data. Recently, it has been shown [16.16] that both strategies may be combined. A weighted maximum-likelihood expectation-maximization (MLEM) approach can be used to reduce the influence of the residual inconsistencies from interpolation in such a way that optimal imaging quality is obtained by optimizing the compromise between residual inconsistencies and data voids.

Motion Artifacts

So far it has been assumed that the morphology in the slice to be reconstructed does not change during data acquisition. However, if one also has to take into account the temporal variation of the attenuation coefficient $\mu = \mu(\xi, \eta, E, t)$, one faces the problem of image reconstruction with a changing data basis; that is, the data measured during the rotation are inconsistent. As a countermeasure, one fundamental goal for engineers developing new CT scanner generations is the acceleration of data acquisition, particularly with respect to the time constants related to anatomical and physiological motions. The presently used scanners are multislice subsecond CTs, which, however, are not able to display perfect radiographs of beating hearts without electrocardiogram (ECG) triggering.

Sampling Artifacts

As in general in any signal processing task, Shannon's sampling theorem must not be violated in CT. This applies to both the reconstruction of an axial slice and the subsequent reconstruction of three-dimensional (3-D) data presentations by slice stacking (Sect. 16.5.3). Subsampling of a signal also results in the typical aliasing artifacts. An inherent sampling problem discussed in [16.4] arises particularly for a detector array with a rectangular sensitivity profile of the single detector elements, namely that the individual elements would have to be arranged at half the distance of their own width. As this requirement cannot be met due to obvious technical reasons, one makes use of an elegant mechanical trick. The corrective action, which is nowadays used to prevent aliasing, is based on either the quarter detector shift or the so-called *flying focus* of the x-ray tube.

Electronic Artifacts (Ring Artifacts)

There are several electronic defects that can deteriorate the image and in most cases destroy it. The most famous, or rather notorious, electronic defect is the failure of a detector channel. In third-generation CT scanners, such a detector defect will result in prominent so-called ring artifacts. As the x-ray source and the detector array are tightly joined at the sampling unit, the failure of an individual detector element, or the corresponding processing channel, becomes specifically visible. During the filtered backprojection the virtual lines connecting the corresponding detector element and the x-ray source, which are sometimes called defective beams, form the tangents of a circle. This means that all values outside the circle are seriously affected by this artifact. Inconsistencies with the measured values of the corresponding other projection directions in fact arise for each point of each line. Due to the backprojection, all image areas are again affected by the artifact.

Scatter Artifacts

For the detector element located in the unscattered, direct beam path, in principle it does not make any difference which physical mechanism of interaction actually reduces the intensity. Other detector elements located outside the direct line of sight may in fact be impaired by certain interactions. Particularly in the area of strongly attenuating anatomical objects such as the shoulder, abdomen, and pelvis, the measured values may be distorted due to scattered radiation. These scattered x-rays may become a considerable part of the overall signal. Whereas the scattered radiation is almost the same for all projection angles, it is very different for the wanted signal. In projection directions in which highly absorbing objects are located one after another, the wanted signal may become extremely weak, so that the scattered radiation dominates the signal. Within the filtered backprojection, inconsistencies then arise from this projection direction, which result in streak artifacts. With regard to the interfering radiation caused by scattering reaching the detector, third-generation CT scanners are superior to fourth-generation CT scanners. The detector array of such scanners is designed such that the row of detector elements is arranged on a circular segment with the x-ray source located at the circle center. It is therefore possible to collimate the radiation by septa so that scattered radiation – with an incident angle into a *false* detector element, which is larger than a threshold angle – is effectively shielded. The critical angle is determined by the length and the spacing of the detector segments. In fourth-generation scanners the detectors are located on a circle, the center of which is the isocenter of the measurement field. An x-ray source, to which a detector collimation might be focused on successfully, obviously cannot be located there.

16.5 Scan Planning and Applications

In the following sections, some important practical aspects of computed tomography (CT) will be discussed. Among others, these aspects concern scan planning, data processing, and representation – particularly gray value scaling. In particular, scan planning plays an important role in clinical applications of CT, since scans cannot be arbitrarily repeated due to the system-inherent radiation dose to which the patient is exposed.

Therefore, it is furthermore not only important to plan the scan properly, i. e., to prepare the image acquisition, but also to be informed about how the image data may be represented, i. e., how to postprocess the acquired data appropriately to maximize the information that is available from the images by means of modern visualization techniques.

16.5.1 Scan Planning

The first and most important step in planning a CT scan is the acquisition of an overview scan, which is called a topogram (Siemens), scanogram (Philips), scout view (General Electric) or pilot scan by the different manufacturers. To acquire this overview scan, the rotation of the sampling unit is stopped at a desired angle. In principle, any angulation is possible, but typical positions are *anterior–posterior* (a.p.), i. e., x-ray examination from the patient's front to the patient's back, and *lateral*, i. e., x-ray examination from the side.

During acquisition of the overview scan, the patient table is continuously moved through the measuring field. Figure 16.7a exemplarily shows images resulting from an a.p. and a lateral overview scan. The resulting images are quite similar to conventional x-ray images. However, both imaging techniques differ in that a parallax in the axial direction of the patient does not occur for the overview scan because of the minimal divergence of the x-ray beam due to slice collimation.

By means of the a.p. overview scan, it is possible to plan and program a particular slice plane, the slice thickness, and the number of slices or the volume. When using the lateral overview scan it is also possible to program special slice orientations by appropriately tilting the entire gantry. This is especially useful in skull radiographs and spinograms to exclude sensitive organs (e.g., eyes) from the scan. Figure 16.7a shows an a.p. overview scan of a thorax. Here, axial slices with a thickness and distance of 8 up to 10 mm are typically scanned. If the lumbar vertebrae are to be examined, the gantry must be tilted such that it is adapted to the orientation of the individual vertebral bodies. Figure 16.7a also highlights that this is the only possibility for acquiring planar images of, for instance, the intervertebral disks.

Figure 16.7b,c shows two different orientations of the skull. If one aims to acquire coronal skull images, it is necessary to place the patient appropriately on the table. In Fig. 16.7b, a lateral overview scan of the patient can be seen. The patient is lying on his abdomen with his head heavily hyperextended. This hyperextension of the head is indeed required due to the limitations in the angle of gantry tilt. Two tomographic slices are shown on the right in Fig. 16.7b. Such radiographs are frequently used either to diagnose chronic sinusitis or to evaluate bone fractures. In slice 1, artifacts due to dental fillings can clearly be identified. Slice 2 shows a section of the frontal calvarium of the skull with spongiosa. Both slices allow unobstructed paranasal sinuses to be discerned. In comparison, axial images without gantry tilt are shown in slices 3 and 4 of Fig. 16.7c.

16.5.2 Hounsfield Units and Gray-Value Mapping

In CT, the attenuation values μ from (16.1) are usually represented as gray values. In this context, an approach developed by Hounsfield has proven to be appropriate and is nowadays commonly used. Here, the attenuation values are transformed onto a dimensionless scale and are related to the attenuation value of water. The definition of these CT values reads

$$\text{CT value} = \frac{\mu - \mu_{\text{water}}}{\mu_{\text{water}}} 1000\,. \tag{16.1}$$

In honor of Hounsfield, the unit of these values

$$[\text{CT value}] = \text{HU} \tag{16.2}$$

is called the Hounsfield unit (HU). On this scale, the CT value of -1000 HU is assigned to air and the CT value 0 HU to water. In principle, this is an open-ended scale, but in practice it ends at ≈ 3000 HU. The range of 4000 HU overall can be captured quite well by means of 12-bit gray-value images. This scaling is arbitrary, but nevertheless has practical consequences. Since the attenuation values of almost all organs – except the bones – are quite similar to those of water, the difference from the attenuation value of water that is given by (16.1) is of per mill.

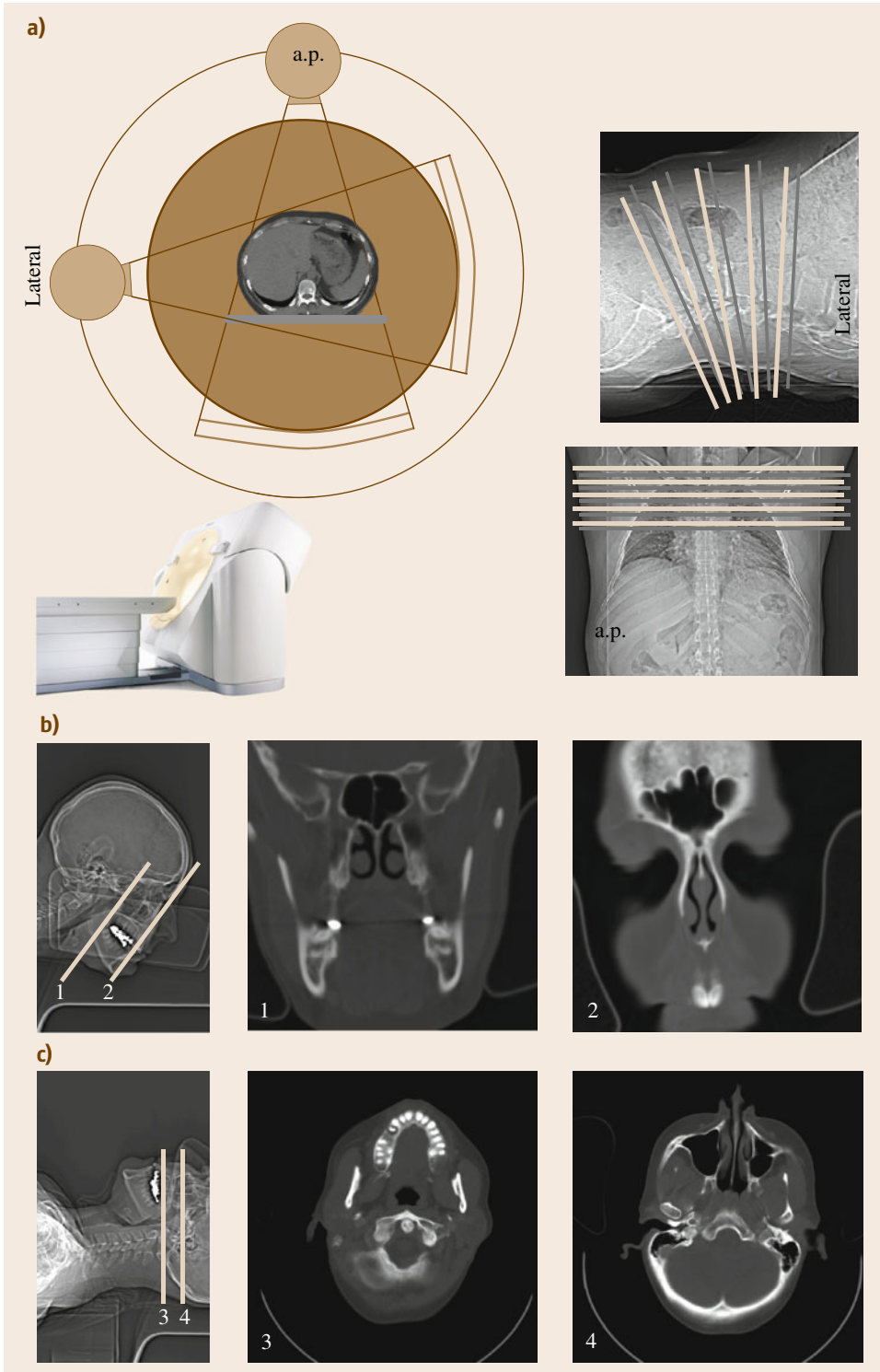

Fig. 16.7a–c Preparation of an overview scan to plan the slice plane position **(a)**. With a fixed tube detector position, the table is continuously moved through the *gantry*. This produces projection images similar to x-ray fluoroscopy. Two geometries are typically used: lateral – the patient is x-rayed from the side; anterior–posterior (a.p.) – the patient is x-rayed from the front to the back. Lateral overview scan for planning the slice position of head tomograms **(b,c)**. Due to the limited tilt of the gantry, the patient has to be bedded face-down and with his head hyperextended to the neck to be able to acquire a coronal representation of the facial cranium (slices 1 and 2). In comparison, axial images without gantry tilt (slices 3 and 4)

Radiologists are accustomed to considering CT values as absolute values which can unequivocally be assigned to the organs. Deviations of these CT values for certain organs indicate pathology. Section 16.4.4 already pointed out the dependence of the x-ray attenuation on the wavelength of the radiation and the potential artifacts arising from this. This problem, which emerges in the case of all CT scanners used for diagnostic imaging, is a consequence of the usage of polychromatic radiation spectra.

While passing through the body, the spectral distribution of the radiation changes such that unequivocal assignment of attenuation values is actually not possible. Nevertheless, the view of the radiologists is largely justified, since most organs behave like water with regard to radiation physics. Therefore, it is possible to correct the beam hardening for these objects by means of a calibration measurement performed with a water phantom. Thus, for the CT values of soft tissue, the definition of the Hounsfield value is directly linked to the tissue density ρ. In this context, Fig. 16.8b is of special interest because different organs and organ changes can be readily distinguished.

It is sensible to divide the whole Hounsfield scale into diagnostically relevant intervals as shown in Fig. 16.8. Figure 16.8a shows a histogram of the relative frequencies of the CT values of an abdominal slice. The accumulations of air, the foam plastic of the patient bed, as well as the fat and the organs can be seen. In the representation of the tomographical slice of the parenchymatous organs, the problem arises that many organs are mapped into overlapping intervals of CT values. Therefore, a sound diagnosis is actually not easy; thus, textures of organs are also important in clinical practice.

The human visual system cannot resolve the complete dynamic range from $-1000\,\mathrm{HU}$ up to $3000\,\mathrm{HU}$ with 4000 gray-value steps. This is the reason why, in practice, gray-value discriminations of only 256 or 512 steps are resolved on display devices.

Recent studies have shown that the human observer is able to discriminate between 700 and 900 shades of gray for the available luminance range of current medical displays and in optimal conditions [16.17]. To be able to detect differences between organs that have rather similar visual representations in their attenuation, it is necessary to map the respective anatomically sensible Hounsfield interval appropriately to the perceptible gray-value range. For this, one uses the piecewise linear function

$$G = 255 \cdot \begin{cases} 0 \text{ for CT value} \leq \mathrm{WL} - \frac{\mathrm{WW}}{2} \\ \mathrm{WW}^{-1}\left(\text{CT value} - \mathrm{WL} + \frac{\mathrm{WW}}{2}\right) \\ 1 \text{ for CT value} \geq \mathrm{WL} + \frac{\mathrm{WW}}{2} \end{cases} , \tag{16.3}$$

where WW denotes the window width and WL the window level.

Figure 16.8b,c shows the corresponding piecewise linear function for a bone window ($\mathrm{WL} = +300\,\mathrm{HU}$, $\mathrm{WW} = 1500\,\mathrm{HU}$) and a soft tissue window ($\mathrm{WL} = +50\,\mathrm{HU}$, $\mathrm{WW} = 350\,\mathrm{HU}$), as well as their effects on the representation of an abdominal tomogram. Density differences in the spinal process are visible only in the bone window, but differentiation of the soft tissue is hardly possible due to the large width of the window. In the soft tissue window, organs such as the liver and the kidney can be distinguished quite well. However, in this relatively narrow window, all CT values above $+225\,\mathrm{HU}$ are displayed undifferentiated as white areas.

Figure 16.8a also exemplarily shows the results of applying different windows to an image slice of the thorax. Again, the relative frequency of the CT values is given. These images are especially challenging, since lung tissue, soft tissue, and bone tissue might be interesting from a diagnostic point of view. For the classification of the areas, three windows turned out to be quite useful. Thus, the lung or pleura window ($\mathrm{WL} = -200\,\mathrm{HU}$, $\mathrm{WW} = 2000\,\mathrm{HU}$), which allows the lung tissue with its low density to be differentiated, is added to the already mentioned soft tissue window and bone window.

16.5.3 Three-Dimensional Data Representation

In the previous sections, the reconstruction of two-dimensional images has been considered. However, today, medical applications of computed tomography are mainly related to three-dimensional imaging. In a first step, a stack of two-dimensional slices must be acquired. A conventional technique is given by a sequential procedure where the patient, lying on the patient table, is moved slightly in the axial direction of the scanner, i. e., the scanner's z-axis. The table then stops and a complete raw data set of a single slice is measured. The stack of tomogram slices is subsequently used to compute the three-dimensional representation of the depicted anatomy. This procedure is called *secondary reconstruction*.

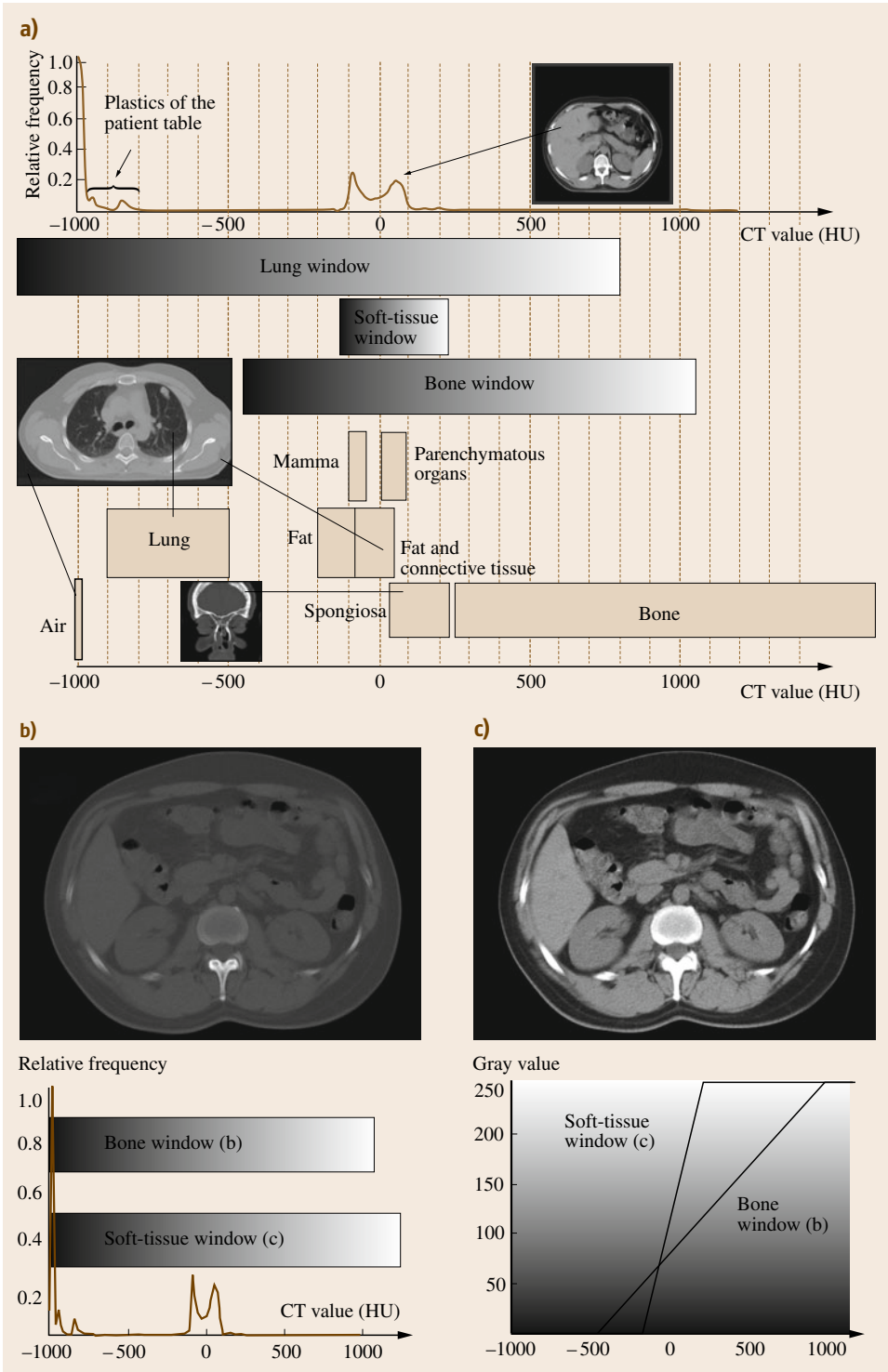

Fig. 16.8a–c Attenuation values in Hounsfield units (**a**). The data are compiled from the collections in [16.18]. The principle of windowing. The complete interval of practically sensible Hounsfield values (HU), ranging from −1000 HU up to 3000 HU (relative frequency of the values for the abdomen area – *lower left*), cannot be recognized and distinguished by the human visual system. Therefore, the different anatomically interesting Hounsfield intervals have to be mapped to appropriate grayscale intervals that can be differentiated. The *lower right* image provides the characteristic curves for two anatomically relevant windows. The *upper* images show the result of the bone window ((**b**): $WL = +300$ HU, $WW = 1500$ HU) and the soft tissue window ((**c**): $WL = +50$ HU, $WW = 350$ HU)

As for the surface visualization method, it is necessary to select a gray value threshold representing the surface. In this context one has of course a certain degree of freedom, as different objects may be visualized as long as their Hounsfield values are clearly different from one another. The gray-value isosurface will then be illuminated with a virtual light source so that the corresponding light reflections can be computed to display the result.

An alternative visualization method of 3-D CT data is multiplanar reformatting (MPR). MPR is used to show angulated sections through the three-dimensional stack of slices. Typically, the principal sections (the sagittal, coronal, and axial slices) are presented to the radiologist. In Fig. 16.9e, a coronal reformatting is shown.

Figure 16.9b,c illustrates the volume rendering technique. This method assigns a physical light reflection and scattering value to each voxel (spatial pixel). The computer is then used to illuminate this *data fog* with a virtual light source and to model the optical impression artificially. To do so, real reflection and scattering of light is simulated. If bones, organs, and contrast-media-enhanced vessels are assigned different optical properties, interesting insights into the pathological status of the patient can be gained. In a postprocessing step, certain tissue types can be suppressed. In Fig. 16.9d, for example, bone is eliminated by a spe-

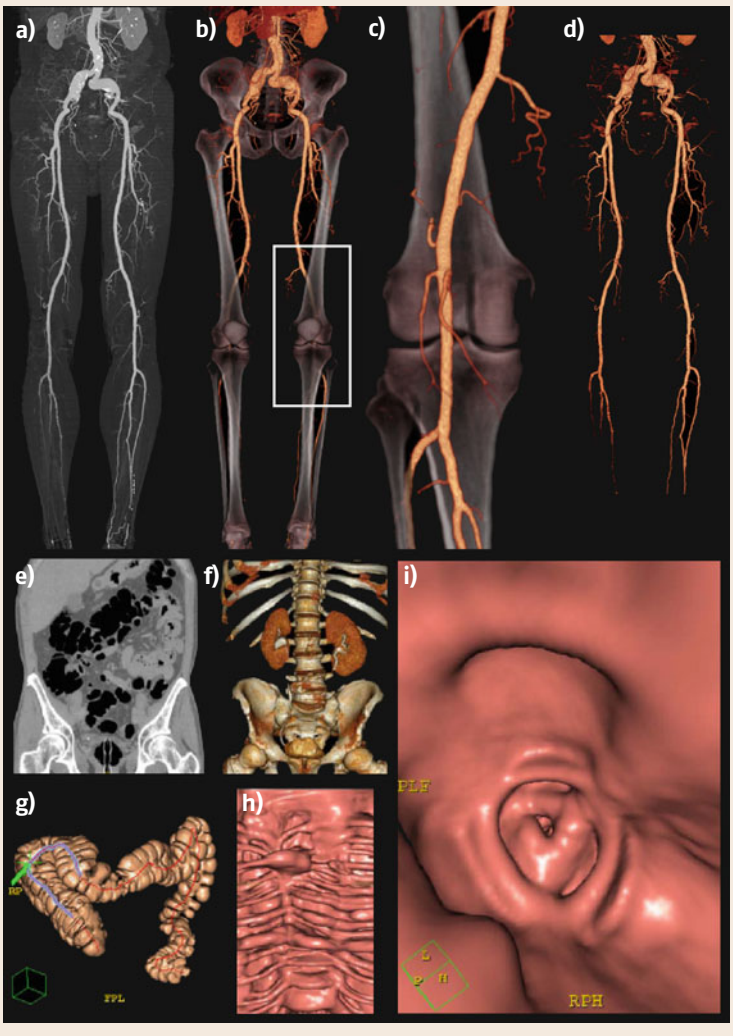

Fig. 16.9 **(a–d)** Angiographic image acquisition with CT (CTA). **(a)** *Maximum-intensity projection* (MIP), **(b)** volume rendering, **(c)** zoom into the knee and visualization from the back, and **(d)** virtual bone elimination with the bone removal technique. **(e–i)** Three-dimensional representation of the abdomen. **(e)** Coronal reformatting, **(f–i)** volume and surface rendering, **(g)** virtual endoscopy of the intestine together with **(i)** the representation of the virtual endoscopy trajectory, and **(h)** virtually opened intestine in cylindrical coordinates

cial bone removal technique for better visualization of the vessel tree.

An alternative to volume rendering is surface rendering, as illustrated in Fig. 16.9f–i. The individual shades of gray of the layers (images) in the data stack represent the degree of physical attenuation of the x-ray beam. In a clinical context, deviations from the normal distribution of these values may indicate pathological changes in the patient.

During visualization, it is possible to visualize certain ranges of values and to selectively suppress others. If the viewer chooses a constant gray value, i. e., a threshold, all spatial points with this value may be displayed in space as an isosurface. This surface is approximated by triangles using a technique called triangulation. Then, the mosaic of triangles is again illuminated and displayed using the virtual method described above. The larger the number of mosaic pieces

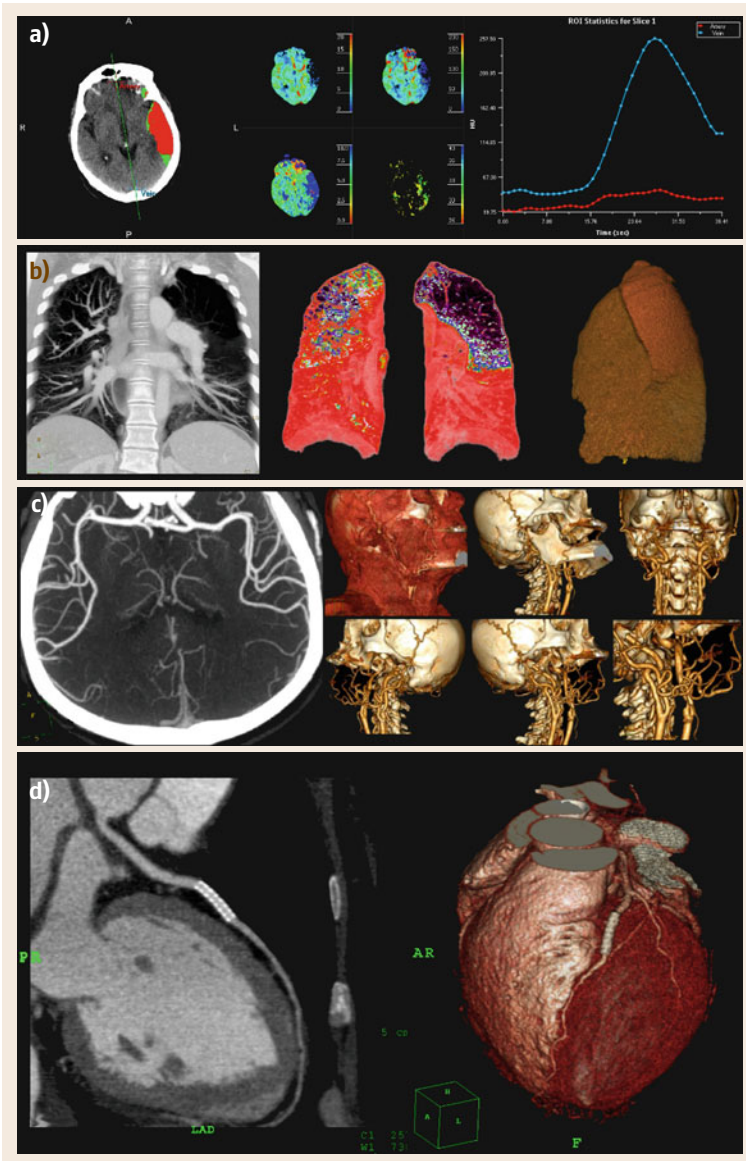

Fig. 16.10 (a) Perfusion measurement for stroke patients, (b) visualization of lung emphysema, (c) CT angiography of the cranial vessels, and (d) imaging of a coronary stent

chosen for the reconstruction of the surface, the more lifelike the result.

In addition to the three-dimensional representation of organs or bone surfaces, which may be interactively rotated on the computer screen, an interior view of hollow organs and airways of contrast-enhanced vessels can be produced. In this way, virtual flights into the body – for example, into the bronchial tubes or the intestine – can be visualized. In Fig. 16.9i, a virtual insight into the human intestine is shown. The value of such a three-dimensional diagnostic approach lies in the reduction of the large amount of data otherwise inherent to the hundreds of single slices.

16.5.4 Clinical Applications

The final section of this chapter describes the broad variety of clinical applications of modern CT imaging by means of some examples. In Fig. 16.10, four typical applications are illustrated. Important fields of application are summarized in the following.

- *Brain perfusion*: The blood flow in the brain (cerebral blood flow, CBF), blood volume in the brain (cerebral blood volume, CBV), mean transit time (MTT), and peak time of the bolus maximum (time to peak, TTP) are acquired and displayed as colored overlays on the relevant CT slices. In this way, colored maps of tissue vitality give indications of an acute or chronic infarct (Fig. 16.10a).
- *Liver perfusion*: Arterial and portal measurements of perfusion in liver studies.
- *Tumor perfusion*: Characterization of known lesions via their perfusion.
- *Lung measurement*: Diagnostics of lung emphysema (Fig. 16.10b); automatic detection of lung nodules.
- *Calcium scoring*: Quantification of coronary calcification.
- *Vessel analysis*: Visualization of vessel trees (Fig. 16.10c); analysis of stenoses and aneurysms; planning of stents.
- *Cardio CT*: Identification and quantification of stenoses; planning of stents and visualization of implanted stents (Fig. 16.10d).
- *Virtual endoscopy*: Three-dimensional CT data as a basis for anatomical interior views of hollow organs (Fig. 16.9i) and contrast-enhanced vessel trees.
- *Trauma*: Fast imaging of the entire body for diagnostics of accident injuries.
- *Dental planning*: Three-dimensional reconstruction and slices through the maxilla and mandible as a planning basis for implantation of prostheses for the oral surgeon.
- *Planning of radiotherapy*: Three-dimensional CT reconstruction as a basis for dose planning in the radiation therapy of tumors.
- *Image-guided surgery*: Three-dimensional CT reconstruction as a basis for planning and navigation of surgical interventions.
- *Interventional imaging*: Visualization of a surgical instrument tip during a biopsy.

In particular, perfusion measurements show that today CT is on its way towards becoming a functional modality. This technique allows the blood flow to be measured after contrast media injection into different organs.

16.6 Dose

The gain in diagnostically valuable information accompanying the advent of computed tomography was considered to be exceptional. This is one of the main reasons why the applied dose was not considered to be of vital importance during this developmental stage. Based on the number of devices currently installed in Germany and an average of 3500 examinations per year, an annual total number of several hundreds of millions of slices can be estimated to be acquired each year.

This approximately lies within the same range as the total number of standard projection radiographs acquired in clinical practice. Considering the different types of radiological examinations (x-ray examinations), one immediately becomes aware of the following discrepancy. Although CT examinations represent only about 4% of all radiological examinations, their share of the total dose amounts to $\approx 35\%$. In short, CT accounts for the largest portion of medically related x-ray exposure.

Considering new generations of CT scanners, such as spiral multislice CT, the applied dose indeed is not reduced. In fact, it is more likely that the dose applied during one single imaging session will increase. This is mainly due to the fact that, in modern

scanners, longer sequences and thinner slices can be easily measured [16.19]. Initiated by reports about unnecessarily high x-ray exposure in pediatric CT examinations [16.20], which were actually performed on the basis of the same scanning protocols as were used in human adults, a high sensibility concerning the applied dose has emerged among both manufacturers and users. Recent developments such as automatic exposure control take the problem of dose into account. With this technology, one can easily adjust the dose according to the anatomy of the patient or likewise take into account whether the individual under examination is an adult or an infant.

Figure 16.11a schematically illustrates that one initially has to differentiate patients according to their physique and between infants and adults. If we adopt the same tube current–time product for infants as is used in scan protocols for adults (Fig. 16.11a, left), the obtained intensity of the x-ray at the detector and thus the applied dose, with respect to the achievable diagnostic quality (i. e., the SNR $= \mu/\sigma$), is unnecessarily high. Therefore, in the case of a pediatric examination, it indeed is reasonable to decrease the anode current to a level that allows a comparable diagnostic quality to be obtained as achieved in the examination of an adult (Fig. 16.11a, right). Such automatic exposure control (AEC) can be steered by means of the scanogram.

Figure 16.11b illustrates dynamic adaptation of the x-ray tube current or dose with respect to the anatomical situation observed along the axial z-axis (longitudinal dose modulation). In anatomical areas in which, as known a priori, low attenuation of the x-ray intensity is to be expected (for example, within the lung area) the tube current and thus the dose can be lowered, without decreasing the image quality. If all areas are imaged with the same tube current, this will result in either dose rates that are too high or noise levels that are too strong.

Figure 16.11c illustrates dynamic adaptation of the tube current across the projection angle γ to the integral attenuation of the radiated body area (angular dose modulation). At all sections through the body, which are oval rather than circular, the angular dose modulation is to be applied. In particular for image acquisitions of the shoulder, strong dose modulation is to be used.

Another possibility for dose reduction arises in cardiac imaging. In Fig. 16.11d, a trigger sequence of an ECG-triggered image acquisition of the heart is depicted. Since data are only acquired within the resting phase of the beating heart, the overall dose can be significantly reduced, provided that the tube current is switched off outside the data window. This effective and efficient procedure is called temporal dose modulation. Figure 16.11e shows the effect of the combination of longitudinal and angular dose modulation on the attenuation of the x-ray beams and on the tube current.

Apart from device-related measures for reduction of radiation exposure, for which the manufacturers bear responsibility, there is a set of user-related measures which also affect the applied dose. The quantities and their connection to the dose, adjustable in the scan protocol, are given in the following. For a detailed discussion on radiation exposure in CT, one is referred to the book by *Nagel* [16.19].

- *Current–time product (mAs product)*: Dose and mAs product, i. e., the product between the x-ray tube current and acquisition time, have a linear dependence. However, the standard deviation, i. e., the image noise, increases proportionally to the inverse of the square root of the mAs product.
- *Acquisition time*: At constant x-ray tube current, the dose increases linearly with acquisition time. However, the mAs product is always to be considered as a total, so that, at a constant dose, the acquisition time can be reduced along with simultaneously increasing the tube current. Thereby, the image noise is unaffected; however, motion artifacts are less likely to occur at short acquisition times (Sect. 16.4.4).
- *Tube voltage*: With increasing tube voltage U_a (Sect. 16.3.1), the efficiency of the x-ray tube as well as the penetration of the radiation are increased. The intensity of the radiation increases with U_a on average following a power of 3.5. With deeper penetration of the radiation, the image contrast obviously decreases. However, this is more than compensated for by the better quantum statistics. Therefore, the image quality generally is improved – obviously at the expense of a higher dose being applied to the patient. If the voltage is, for instance, increased from 120 to 140 kV, in order to reduce the dose whilst maintaining image quality, the mAs product must be reduced by 40%. Thus, a dose reduction of $\approx 15\%$ is obtained [16.19].
- *Thickness of the object to be imaged*: For infants and frail patients, one has to bear in mind that a smaller mAs product has to be adopted. Due to lower attenuation, the statistics of the x-ray quanta are still as good as for adults or heavier patients. Correspondingly, image quality is not affected. For heavier patients, an increase in x-ray tube voltage is prefer-

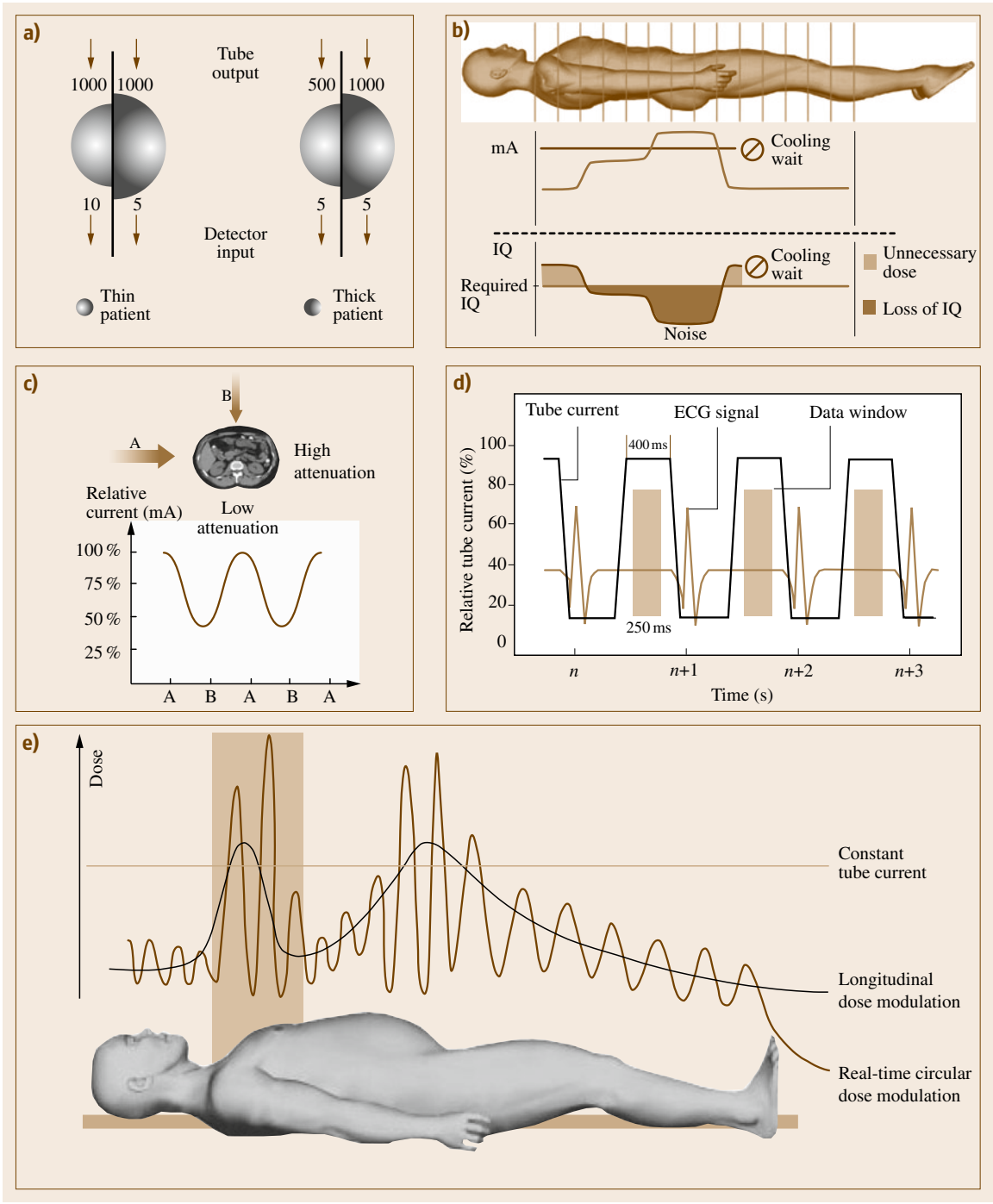

Fig. 16.11a–e Active methods for dose reduction [16.19]. **(a)** Automatic exposure control (AEC) differentiates between heavier and thinner patients. **(b)** The longitudinal dose modulation – a dynamic adaptation of the tube current or dose to the anatomical situation. **(c)** Angular dose modulation – a dynamic adaptation of the tube current or dose to the shape of the axial body section. **(d)** Temporal dose modulation. **(e)** Combination of longitudinal and angular dose modulation. (IQ – image quality)

able to an increase in the mAs product, since the increase in radiation exposure is less intense.

- *Slice thickness*: The slice thickness can typically be adjusted by means of a tube sided collimator from 1 up to 10 mm. Thereby, the slice thickness does not affect the dose if the same body section is to be measured. The advantage of a finer slice sequence is the reduction of partial-volume artifacts as well as step artifacts occurring on coronal or sagittal reformatting of the image. The disadvantage is that, at a finer collimation, fewer x-ray quanta will reach the detector such that the image noise will correspondingly increase. If the image quality is to be kept constant, the mAs product and thus the dose will have to increase inversely proportionally to the slice thickness.
- *Pitch factor*: A pitch factor of $p = 1$ means that, in the case of a rotation of the sampling unit through 360°, the patient table is moved linearly by a length equal to the adjusted slice thickness (Sect. 16.4.3). If $p < 1$, the individually measured slices have a larger overlap, such that the image quality is increased. However, this results in an increased dose. Accordingly, if $p > 1$, the dose can be reduced. In theory, an artifact-free image reconstruction should be possible up to a pitch of $p = 2$. With this, the scanning length is increased such that, for the same mAs product, fewer x-ray quanta are available for the image formation of a coevally larger body section. Therefore, the image noise increases.
- *Scanning length*: If the imaged body section is enlarged, the dose applied to the patient will increase accordingly. This is expressed by means of the effective dose or the dose–length product. The number of slices always has to be limited to the diagnostically relevant section, which has to be specified in the overview scan (Sect. 16.5.1).
- *Filter kernel*: The choice of the respective filter kernel at first glance does not directly influence the dose. However, as described in Sect. 16.4.2, the choice of the high-pass filter of the filtered backprojection does indeed affect the image resulting from the reconstruction, since the choice of the filter kernel represents a trade-off between noise and spatial resolution. If one wants to reduce the noise while maintaining high spatial resolution, this is only possible at the expense of an increase in dose. Thus, it always depends on the diagnostic question as to whether an appropriate choice of the filter kernel can be used for dose reduction.
- *Window width*: The window width (Sect. 16.5.2) used for adjusting the display of the CT images does not initially have a direct influence on the dose. However, the higher the contrast selected by constricting the window width, the stronger the noise present in the images. Conversely, it is possible to smooth the image by enlarging the window width. If there is a contrast reserve due to the diagnostic question, smoothing of the visualization can already be incorporated during the planning step. This will decrease the mAs product and thus the radiation exposure.
- *Field of view (FOV)*: When using a very small FOV, i. e., a very strong detail magnification, as a general rule, a very sharp reconstruction filter has to be used. This is due to the fact that the magnification of the section under examination is chosen because a locally more detailed image needs to be analyzed. This immediately has consequences for the image noise, which can only be reduced with an increase in the mAs product and, therefore, an increase in the applied dose.

Finally, it should be mentioned that the progress toward smaller detector elements also influences the dose. It can be shown that, for constant signal-to-noise ratio, the dose increases with the inverse fourth power of the detector element size, as described in detailed in [16.4]. If in the formula of Brooks it is assumed that $b = d = \Delta\xi$ for the sampling distance at the center of rotation and for the slice thickness, respectively, then, in consideration of the definition of the signal-to-noise ratio $\mathrm{SNR} = \mu/\sigma$, one obtains the relation $D \propto (\mathrm{SNR})^2/(\Delta\xi)^4$. Obviously, this limits a further reduction of the size of the detector elements, since the dose may not be arbitrarily increased.

16.7 Special System Designs

In the last few decades, special CT imaging designs have been developed for certain applications, and this chapter concludes with a brief review of five of these. For coronal imaging, the problem of motion artifacts (Sect. 16.4.4) arises with the conventional CT imaging concepts described above. Third-generation CT systems

therefore require ECG-triggered data acquisition, because with respect to the time constants of heart motion, even subsecond CT scanners without ECG-triggered data acquisition are too slow.

For this kind of clinical application, electron-beam computed tomography (EBCT) has been developed and will be described below in Sect. 16.7.1. Furthermore, a short description of volume or cone-beam CT – often abbreviated as VCT or CBCT, respectively – will be given in Sect. 16.7.2. These systems are subsequent steps beyond multislice CT (MSCT). However, if very small object details in the micrometer range must be imaged, the spatial resolution of conventional clinical CT is insufficient. For this task, special micro-CT systems have been developed (Sect. 16.7.3). Since nuclear imaging is able to visualize the metabolism of a patient, and x-ray transmission computed tomography gives complementary morphological information, a consequent idea is the combination of both modalities into so-called PET-CT scanners, which will be introduced in Sect. 16.7.4. In the last section (Sect. 16.7.5), a system extension to include two sampling units, i. e., two x-ray tubes and two corresponding multislice detector arrays in a so-called dual-source system, is described.

16.7.1 Electron-Beam CT

If there is a need for extremely short acquisition times, the concept of moving sampling systems must be left behind entirely. One approach to achieving this is the use of electron-beam computerized tomography (EBCT). This type of CT was developed for cardiac imaging.

In EBCT, there is no longer a localized x-ray tube rotating around the patient as in conventional CT technology. Instead the patient is situated, in a manner of speaking, *inside* the x-ray tube. An electron beam is focused onto wolfram target rings, which are arranged in a half circle around the patient, and generates the desired x-ray fan beam upon impact with the wolfram target. The x-ray irradiation is measured with a stationary detector ring. Such systems have mainly been sold to cardiologists by the company Imatron. The electron-beam technique is able to acquire an image slice in 50 ms. Figure 16.12a shows a diagram of an EBCT system as well as an illustration of a modern Imatron system. Further technical details can be found in [16.22].

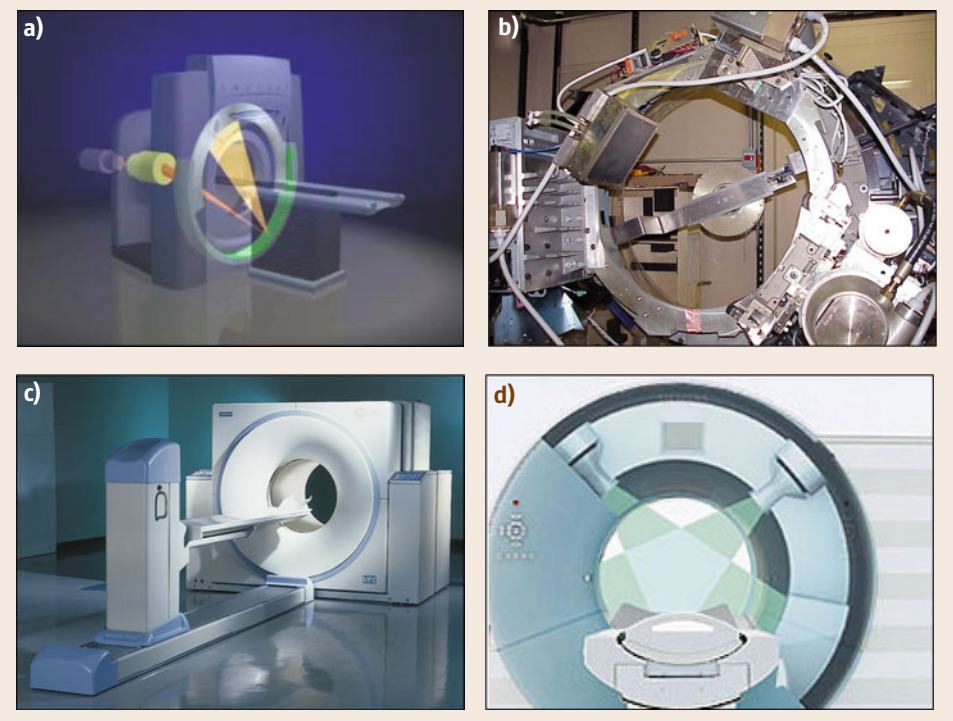

Fig. 16.12 (**a**) Electron-beam CT, (**b**) volume or cone-beam CT, (**c**) PET-CT, and (**d**) dual-source CT [16.21]

16.7.2 Volume CT

There has so far not been a common definition of the generations of development of CT. In [16.10], scanners equipped with a cone-shaped x-ray beam and a plane detector are referred to as the seventh generation. However, even within the cone-beam scanner itself, one needs to distinguish between systems that use only a small cone opening, as in the case of a multislice (multiline) detector system or indeed a symmetric x-ray cone. In particular, the necessary reconstruction methods differ extensively between these systems. To understand the motivation behind the development of cone-beam CT systems, recall that the step from the pencil-beam to the fan-beam concept came along with the advantages that the x-ray source was exploited more effectively, and that there was a reduction in acquisition time. The efficiency of the energy transformation in the generation of x-ray radiation is just about 1%.

As the heat produced inside the x-ray tube essentially defines the physical capacitance, and therefore limits the measuring time, the next straightforward step in the development of CT scanners involved the use of a cone-shaped x-ray beam, which is already produced in the x-ray tube. Both the pencil-beam and the fan-beam geometry are created by means of appropriate pinhole or slit collimators, which reshape the original x-ray source intensity profile, reducing efficiency.

Technologically, there are three important problems that had to be solved before the successful application of cone-beam geometry to CT imaging. First of all, a flat-panel detector, which did not exist at the time, had to be introduced to replace the line or multiline detector arrays. Second, the huge amount of raw data that quickly emerge on subsecond scanners in particular had to be transferred from the rotating sampling unit to the image reconstruction computer. The bandwidth required for the data transfer poses a challenge even today. Third, there is the problem of reconstruction, whose mathematics is slightly more sophisticated compared with the two-dimensional methods.

Figure 16.12b schematically shows the cone-beam geometry of an imaging system with a planar detector (flat-panel detector, Sect. 16.3.2). The planar detector geometry was first applied for technical applications in micro-CT, since the required charge-coupled device (CCD) chips were only available for this geometry. Figure 16.12b shows a prototype of a so-called volume CT (VCT) developed by General Electric Medical Systems.

16.7.3 Micro-CT

Recently, micro-CTs, which essentially comprise a miniaturized design of the cone-beam CTs mentioned in the previous section and which are typically used for nondestructive, three-dimensional microscopy, have become commercially available. The x-rayed measuring field, often as small as $2\,\mathrm{cm}^3$ in volume, is so small that medical applications might seem to be ruled out. Indeed, these scanners are more commonly used for material testing and analysis, but medical applications are on their way to taking center stage. An example in human medicine is the analysis of trabecular structures in bones. Micro-CTs are also ideal scanners for radiological examinations of small animals [16.23]. Micro-CTs are often produced as desktop devices and have a measurement chamber that is entirely shielded by lead walls against scattered x-ray beams, so that no further means of protection are necessary. The object to be examined is placed on a rotating specimen disk, which is controlled by a stepper motor.

The two most crucial components of micro-CTs are the x-ray tube and the two-dimensional detector array. In particular, it is the size of the focus and the size of the detector elements that, apart from the mechanical accuracy of the rotary motion, determine the spatial resolution. Therefore, micro-CT systems need a microfocus x-ray tube. An x-ray focus size of $b_\mathrm{F} < 10\,\mu\mathrm{m}$ is desirable. Unfortunately, when using such a small target area for the electrons, the anode current cannot be very large. The current is typically less than $100\,\mu\mathrm{A}$. Since the current controls the intensity of the x-ray spectrum, there are certain constraints with respect to the materials being examined.

A 12-bit x-ray charge-coupled device (CCD) chip with a pixel matrix of 1024×1024 or higher may be used as a detector, which can be connected to a scintillation crystal by fiber optics. The size of the picture elements typically has an order of magnitude of around $b_\mathrm{D} < 10\,\mu\mathrm{m}$. SkyScan specifies a resolution of about $10\,\mu\mathrm{m}$. As micro-CTs are cone-beam x-ray systems, three-dimensional reconstruction methods are required to calculate the images [16.24].

16.7.4 PET-CT

With the exception of contrast-enhanced angiography and perfusion techniques, CT, on its own, is only able to provide morphological information, i. e., information on the shape of objects. On the other hand, positron emission tomography (PET) provides informa-

tion on metabolism, i. e., the biomedical function of an anatomical region [16.25]. CT, however, is based on the attenuation of x-ray radiation. Different organs, having different absorption properties, are therefore only imaged according to their shape, and the patient is considered to be passive during imaging.

In PET, the patient is injected with a radioactively marked *tracer*, which is metabolized inside the body. One very important tracer is 2-(fluorine-18)-fluoro-2-desoxy-D-glucose (^{18}F-FDG), which can be used to trace glucose metabolism. This is especially important for oncology studies, since, due to their faster metabolism, the ^{18}F-FDG uptake of tumors exceeds the uptake of nonmalignant tissue. Compared with ordinary glucose, ^{18}F-FDG differs in the presence of the tracer atom. As such, it behaves like glucose only at the beginning of the metabolic chain. Thereafter, the molecule is detected but not catabolized any further, leading to an accumulation of the tracer inside the tumor.

^{18}F-FDG is a positron emitter, so wherever the tracer accumulates, the process of positron annihilation is intensified; i. e., upon collision with an electron, the positron entirely dematerializes, becoming two gamma-ray photons that fly away in opposite directions. These gamma-ray photons are then measured by two detectors, located opposite each other, in what is called a coincidence measurement. By means of, for instance, filtered backprojection or statistical reconstruction, the location of the dematerialization can be reconstructed, and tumors are represented as *hot spots* inside the image.

An interesting approach to imaging diagnostics is the combination of both morphological and functional imaging methods. The goal of displaying function along with morphology in a single image has been realized for some time using methods of image registration. Registration is an image processing step that must overcome problems caused by the different positioning of the patient in the two different scanners and changes resulting from the time that passes between the two acquisitions.

In the case of combined techniques, the patient is successively scanned using the different imaging modalities. Using a combined PET-CT scanner, such as, for instance, the *biograph* from Siemens (Fig. 16.12c), the images are acquired almost simultaneously, with the patient effectively in the same position, so that the location of a tumor relative to the surrounding anatomy can be displayed immediately.

16.7.5 Dual-Source CT

Figure 16.12d shows a recent development in the field, the so-called dual-source CT. Two complete sampling units, both of which consist of an x-ray tube and a detector array, are installed perpendicular to each other. Best images of the beating heart are obtained when the acquisition interval is set to the diastolic phase. Since the patients are usually agitated, this resting phase of the heart is often so short that motion artifacts are inevitable. Usually, images have to be acquired across 180°, in order to obtain a complete raw dataset within the relatively short resting phase of the heart. However, when employing a sampling unit taking advantage of the dual-source technology, only a rotation of about 90° is necessary. Thereby, the sampling time is halved, such that motion artifacts are significantly reduced. If one wants to abandon the administration of beta blockers, which are used to lower the pulse, artifact-free image reconstruction by means of a single source scanner is no longer possible. Here, the strength of the halved acquisition time becomes apparent. Using these modern dual-source subsecond scanners a temporal resolution can be achieved that only differs by a factor of 2 from the acquisition speed achieved by electron-beam CT. Considering the applied dose, the ECG-supported triggering of the acquisition window is of great importance. Here, compared with the standard CT scan protocol in which the tube current is not modulated, a dose reduction of up to 50% can be achieved.

References

16.1 E. Seeram: *Computed Tomography* (Saunders, Philadelphia 2001)

16.2 J. Hsieh: *Computed Tomography* (SPIE, Bellingham 2003)

16.3 W.A. Kalender: *Computed Tomography* (Publicis, Munich 2005)

16.4 T.M. Buzug: *Computed Tomography* (Springer, Berlin, Heidelberg 2008)

16.5 G. Grossmann: Procede et dispositif pour la representation radiographique des sections des corps, French Patent 771887 (1934)

16.6 W. Härer, G. Lauritsch, T. Mertelmeier, K. Wiesent: Rekonstruktive Röntgenbildgebung, Phys. Bl. **55**, 37 (1999), (in German)

16.7 W. Härer, G. Lauritsch, T. Mertelmeier: Tomographie – Prinzip und Potential der Schichtbildver-

fahren. In: *Handbuch diagnostische Radiologie*, ed. by T. Schmidt (Springer, Berlin, Heidelberg 2003), (in German)

16.8 G.M. Stevens: Volumetric tomographic imaging. Ph.D. Thesis (Univ. Stanford, Stanford 2000)

16.9 G.N. Hounsfield: Computerized transverse axial scanning (tomography). I. Description of system, Br. J. Radiol. **46**, 1016 (1973)

16.10 J.T. Bushberg, J.A. Seibert, E.M. Leidholdt, J.M. Boone: *The Essential Physics of Medical Imaging* (Lippincott Williams Wilkins, Philadelphia 2002)

16.11 W.A. Kalender, W. Seissler, P. Vock: Single-breath-hold spiral volumetric CT by continuous patient translation and scanner rotation, Radiology **173**, 414 (1989)

16.12 K.M. Mudry: X-ray. In: *The Biomedical Engineering Handbook*, Vol. 1, ed. by J. Bronzino (CRC, Boca Raton 2000) pp. 61–1

16.13 W.A. Kalender: Der Einsatz von Flachbilddetektoren für die CT-Bildgebung, Radiologe **43**, 379 (2003)

16.14 G. Brunst: High resolution digital flat panel detectors for x-ray applications – Basics. In: *Medical Imaging*, ed. by W. Niederlag, H.U. Lemke (Health Academy, Dresden 2002) p. 63

16.15 J. Radon: Über die Bestimmung von Funktionen längs gewisser Mannigfaltigkeiten, Ber. Verh. Sächs. Akad. Wiss. Leipz. Math. Nat. Kl. **59**, 262 (1917)

16.16 M. Oehler, T.M. Buzug: Statistical image reconstruction for inconsistent CT projection data, Methods Inf. Med. **3**, 261 (2007)

16.17 T. Kimke, T. Tuytschaever: Increasing the number of gray shades in medical display systems – How much is enough?, J. Digit. Imaging **20**, 422 (2006)

16.18 E. Krestel (Ed.): *Imaging Systems for Medical Diagnostics* (Siemens, Berlin 1990)

16.19 H.D. Nagel (Ed.): *Strahlenexposition in der Computertomographie*, 3rd edn. (CTB, Hamburg 2002)

16.20 S. Sternberg: CT scans: A very high-dose diagnosis, USA Today **Nov. 20** (2000)

16.21 Siemens Medical Solutions: *Excellence in CT*, *SOMATON Definition*, *Computed Tomographie* (Siemens Medical Solutions, Forchheim 2005)

16.22 G. Weisser: Technische Grundlagen der EBCT. In: *MR-Angiographie und Elektronenstrahl-CT-Angiographie*, ed. by J. Gaa, K.-J. Lehmann, M. Georgi (Thieme, Stuttgart 2000) p. 145

16.23 N.M. De Clerck, D. van Dyck, A.A. Postnov: Noninvasive high-resolution µCT of the inner structure of living animals, Microsc. Anal. **1**, 13 (2003)

16.24 G. Wang, S. Zhao, P.-C. Cheng: Exact and approximate cone-beam x-ray microscopy. In: *Modern Microscopes I*, ed. by P.C. Cheng, P.P. Huang, J.L. Wu, G. Wang, H.G. Kim (World Scientific, Singapore 1998)

16.25 J. Ruhlmann, P. Oehr, H.-J. Biersack (Eds.): *PET in der Onkologie – Grundlagen und klinische Anwendung* (Springer, Berlin, Heidelberg 1998)